Available online at www.sciencedirect.com

ScienceDirect

Journal of Magnesium and Alloys 11 (2023) 1485–1504

www.elsevier.com/locate/jma

Review

Research perspective and prospective of additive manufacturing of biodegradable magnesium-based materials

Qingyun Fu[a,1], Wenqi Liang[b,1], Jiaxin Huang[b], Weihong Jin[b], Baisong Guo[b], Ping Li[a], Shulan Xu[a], Paul K. Chu[c,*], Zhentao Yu[b,*]

[a] *Center of Oral Implantology, Stomatological Hospital, Southern Medical University, Guangzhou 510280, China*
[b] *Institute of Advanced Wear & Corrosion Resistant and Functional Materials, Jinan University, Guangzhou 510632, China*
[c] *Department of Physics, Department of Materials Science and Engineering, and Department of Biomedical Engineering, City University of Hong Kong, Tat Chee Avenue, Kowloon, Hong Kong, China*

Received 13 February 2023; received in revised form 20 May 2023; accepted 24 May 2023
Available online 10 June 2023

Abstract

Biodegradable metals such as magnesium (Mg) and its alloys have attracted extensive attention in biomedical research due to their excellent mechanical properties and biodegradability. However, traditional casting, extrusion, and commercial processing have limitations in manufacturing components with a complex shape/structure, and these processes may produce defects such as cavities and gas pores which can degrade the properties and usefulness of the products. Compared to conventional techniques, additive manufacturing (AM) can be used to precisely control the geometry of workpieces made of different Mg-based materials with multiple geometric scales and produce desirable medical products for orthopedics, dentistry, and other fields. However, a detailed and thorough understanding of the raw materials, manufacturing processes, properties, and applications is required to foster the production of commercial Mg-based biomedical components by AM. This review summarizes recent advances and important issues pertaining to AM of Mg-based biomedical products and discusses future development and application trends.

Keywords: Magnesium-based materials; Additive manufacturing; Wires and powders; Biomedical metallic materials; Medical devices.

1. Introduction

Bone trauma, bone tumors, and skeletal deformities are becoming more prevalent as a result of the aging baby boomer generation and consequently, demand for surgical implants is on the rise globally. Although human bones can regrow, it is difficult for some severe fractures and defects to heal on their own and artificial intervention may be necessary [1]. The mainstream orthopedic implants are normally made of non-degradable metallic materials such as stainless steels [2], cobalt-based alloys [3], and titanium-based alloys [4], which possess higher strength and better physical properties than most medical polymers and ceramics, but can introduce risks such as stress shielding and inflammation [5]. In fact, the roles of surgical implants and devices such as internal fixation plates, bone screws, intramedullary nails, surgical sutures, and vascular stents are temporary, that is, until tissue recovery. In this respect, materials that degrade naturally *in vivo* offer economic benefits and reduce patient trauma because a second surgery to remove the implants can be obviated [6,7].

The ideal orthopedic implants should have mechanical properties resembling those of natural bones in addition to acceptable biocompatibility [8,9]. Furthermore, they must provide sufficient mechanical support while avoiding stress shielding and breaking down at acceptable rates during bone

* Corresponding authors.
E-mail addresses: paul.chu@cityu.edu.hk (P.K. Chu), ninyzt@163.com (Z. Yu).
[1] Both authors contributed equally to this work.

https://doi.org/10.1016/j.jma.2023.05.002

regeneration [10]. Magnesium (Mg) and Mg alloys are desirable biodegradable materials for the following reasons: (1) Safe degradation *in vivo* [11]; (2) Mechanical properties more similar to those of human bones than nondegradable metals such as stainless steels and titanium alloys; (3) Reduction of stress shielding due to mismatch of elastic moduli [12]; (4) Excellent biocompatibility because Mg is one of the essential elements in bone tissues and activates many metabolic enzymes [13]; (5) Excellent osteoinductive and osteogenic properties [14,15].

Nowadays, products of Mg and Mg alloys are commonly processed by casting, forging, and other traditional thermal processing methods [16]. Although the specific strength of the Mg products by traditional manufacturing techniques is quite high, their yield limit are low making them inadequate to support large loads, and casting can produce defects such as cracks and shrinkage [17]. In addition, because of the poor processing properties [18] and low forming efficiency [19], it is difficult to produce complex Mg-based structural products using traditional manufacturing methods. Hence, better manufacturing techniques are highly desirable. Additive manufacturing (AM) of Mg products is of growing interest due to the unique design capabilities AM offers as well as the unknown properties of the materials. Compared to traditional subtractive manufacturing or mold manufacturing, AM has the following advantages: (1) Effective simplification of molding processes and shortening of production cycles; (2) Materials and energy saving, environmental friendliness, and reduction of manufacturing and labor costs; (3) Flexible component structure and shape which would otherwise be difficult by conventional methods [20]. For instance, complex porous structures with both internal and external connectivity can be fabricated using AM technology, which also promotes cell adhesion, proliferation, and bone regeneration in biomedical applications [21,22].

Nevertheless, research on the application of AM to Mg-based products has been limited so far mainly due to the high reactivity of Mg, which leads to uncontrollable oxidation in its pure form and the products must be stored in an environment that prevents exposure to oxygen [23]. Both powders and wires are common raw materials for AM but in these forms, the surface energy is high, thus raising the risk of reacting with atmospheric oxygen and causing combustion. To date, investigations of Mg-based AM products are insufficient. This article provides a comprehensive review of Mg-based AM products from the aspects of raw materials, processing methods, properties, and applications, and future applications and development are also discussed. Our aim is to provide guidance and reference for the application of Mg-based AM products to biomedicine.

2. Raw materials for Mg-based AM

2.1. Powders

Production of Mg powders poses a significant risk of explosion and there are only a few companies engaged in commercial production. Currently, the main products are pure Mg, AZ91D, and WE43 powders. However, owing to the biological toxicity of Al in the AZ91D alloy, only the pure Mg and WE43 powders are suitable for AM of biodegradable Mg-based implants [24]. The preparation methods of Mg powders involve primarily mechanical crushing and atomization techniques. As the optimal particle size range of biodegradable metal implants produced by AM is between 20 μm and 70 μm and the mechanical method produces powders with larger particle sizes, most AM Mg-based powders are produced by gas atomization [25,26].

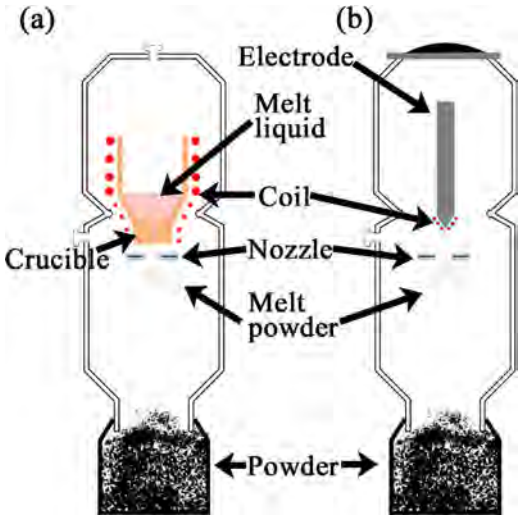

Fig. 1. Schematic of gas atomization equipment: (a) VIGA and (B) EIGA [30].

Gas atomization performed in a high-pressure air stream is employed to break the molten metal stream into small droplets and condense them into powders [27]. Common techniques are vacuum induction melting gas atomization (VIGA) with crucibles and electrode induction melting inert gas atomization (EIGA) without crucibles [28,29]. As shown in Fig. 1, the former is mainly utilized to produce stainless steel and nickel-based alloy powders, while the latter is more suitable for reactive metals such as Mg alloys[30]. Gas atomization has advantages such as high purity, little oxidation, controllable powder size, good sphericity, low environmental impact, and fast cooling, but the preparation process requires protection by argon thus increasing the cost [31,32]. Shanghai Jiao Tong University, in collaboration with Tangshan Weihao Mg Power Co., Ltd., has produced Mg–Nd–Zn–Zr alloy (JDBM) powders by gas atomization. The powders have a smooth surface, excellent roundness, and a particle size range of 50∼75 μm (Fig. 2) [24].

2.2. Wires

On account of the hexagonal close-packed structure, Mg has the limited plastic deformation ability at room temperature. [33]. In order to improve the ductility of Mg-based materials, large plastic deformation is necessary [16,34]. It has been shown that when the heat treatment temperature exceeds

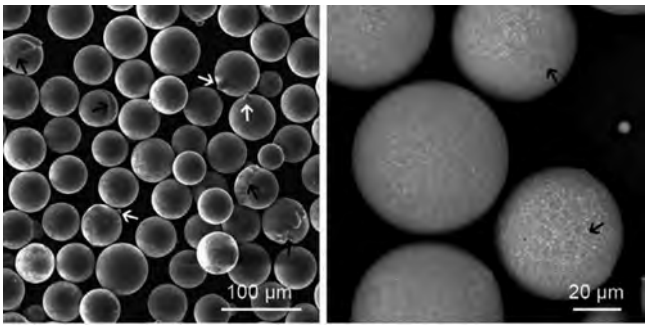

Fig. 2. JDBM powders produced by gas atomization [24].

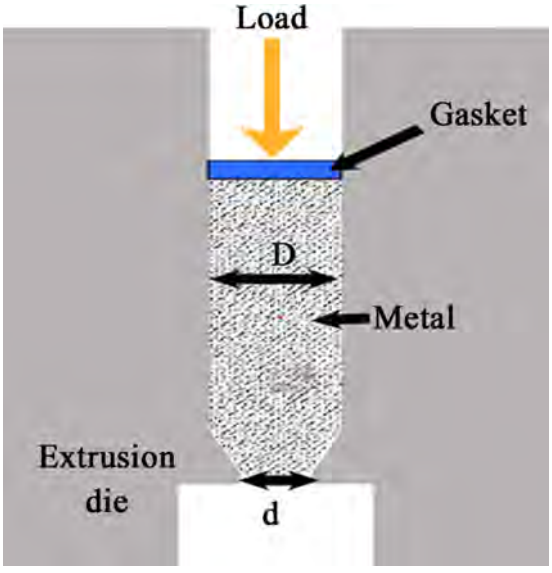

Fig. 3. Hot extrusion device of Mg [37].

220 degrees, additional sliding surfaces will be generated, leading to a brittle ductile transition that improves the plastic deformability [35]. Therefore, Mg and its alloy wires are generally produced by hot extrusion at 300∼500 °C followed by a second precision hot working process at 100∼300 °C. In addition, to produce high-quality and shiny wires, 1∼2 die cold drawing processes at room temperature are required [36].

Hot extrusion is a pressure forming process in which the billet is heated to a certain temperature and forced into a die to form the desired shape as shown in Fig. 3 [37]. The materials in the extrusion zone are subjected to triple compressive stress, so that plastic deformation can be maximized. The conditions in extrusion of metallic materials are not as stringent as those for rolling and forging and hence, hot extrusion is a more suitable for materials with poor plastic deformability at room temperature [38,39]. To create fine Mg wires, drawing processes are usually utilized, as illustrated in Fig. 4 [40,41]. The blank metal is mechanically drawn through a die hole to reduce the cross-section and increase the length. The drawing process has the advantages of high dimensional precision, good surface quality, and simple operation. Some of the Mg alloy wires produced by extrusion and drawing processes are shown in Fig. 5 [42–44].

Mg wires have been used in arc additive manufacturing (AAM) and stacking small quantities of products, welding joints, and repair of large damage. However, the heating source and metallurgical behavior of the materials produced by wire stacking differ from multi-layer, multi-pass stacking AAM thereby creating problems such as poor stacking, spatter, and slagging. Hence, it is necessary to develop Mg wires raw materials with good chemical composition and manufacturing stability for AAM.

3. Technologies for Mg-based AM

In principle, AM is feasible for industrial production of different types of materials including metals, ceramics, and polymers. Metal AM is considered one of the most difficult, albeit promising areas [45] and current mainstream metal additive manufacturing technologies for Mg-based metals are described in this section.

3.1. Laser additive manufacturing (LAM)

LAM has been one of the most extensively researched techniques for Mg alloy products. Because of the minimal divergence and power loss of the laser beam, it can be focused into a small spot (less than 60 μm in diameter), enabling high-precision parts to be produced [46]. LAM includes selective laser melting (SLM, also known as laser powder bed fusion) and laser direct forming (LDF). Due to the use of high-energy direct powder delivery in LDF technology, the melt pool is unstable and therefore, SLM has become one of the widely used LAM technologies [47]. The SLM system is depicted in Fig. 6 [48]. The process involves slicing a three-dimensional model of the part into thin layers with a uniform thickness, converting each layer into a computer numerical code, and using a laser to melt each layer of the powders until the target part is laminated. LAM combines precision and high-performance forming, having the following features: (1) Rapid melting and solidification by the laser, relatively narrow heat affected zone, and forming products with excellent properties and (2) Forming of high-precision parts with precise control, continuous energy transfer, and other important features in terms of space and time [49].

Despite existing reports [50–54] indicating that SLM is an effective method to produce highly complex and high-precision Mg alloy components, SLM of Mg still has the following shortcomings: (1) For the laser heating sources, Mg has low laser light absorption resulting in low energy utilization and working efficiency; (2) Preparation of highly reactive Mg powders is demanding and prone to contamination leading to explosion accidents and higher raw material costs; (3) The inherent properties of Mg and Mg alloys such as the low evaporation temperature, high vapor pressure, flammability, and explosiveness render them susceptible to violet emission during AM, making it difficult to control the chemical composition and morphology of Mg-based metal parts; (4) Mg powders are easily oxidized and the high oxygen content may degrade the mechanical properties of the products if the

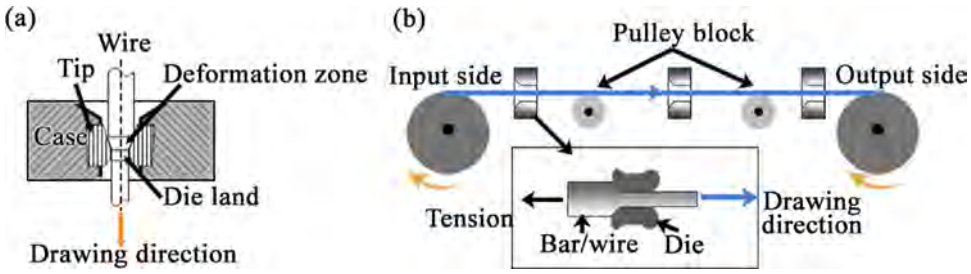

Fig. 4. Schematic illustration of the drawing process of Mg alloy wires: (a) Cross-sectional view of the drawing die [40] and (b) Continuous drawing process [41].

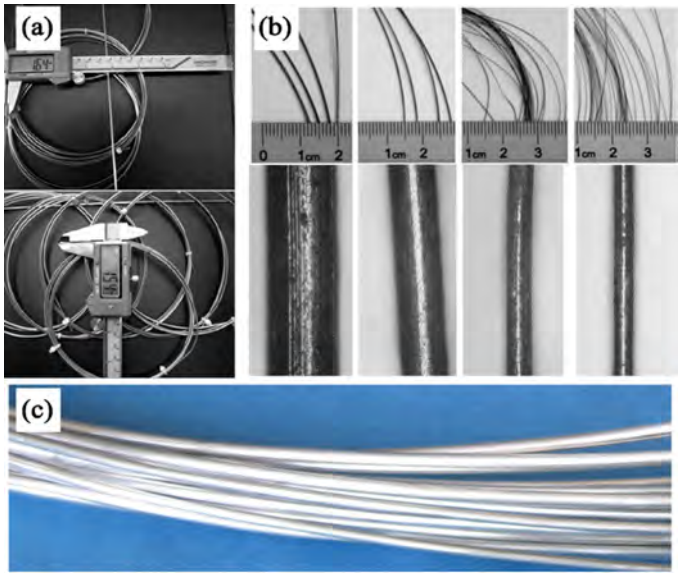

Fig. 5. Mg alloy wires: (a) Mg-6.0%Zn-1.0%Y-0.6%Ce-0.6%Zr wires prepared by the forward extrusion process [42], (b) AZ31 and AZ91 wires prepared by the hot extrusion process [43], and (c) Wires prepared by drawing of MgCa0.8 in a heated die [44].

LAM process such as SLM is not carried out correctly. Therefore, it is important to mitigate oxidation of Mg powders and understand the corresponding relationship.

3.2. Electron beam additive manufacturing (EBAM)

In EBAM, a high-energy electron beam melts the metal (powders or wires) under vacuum conditions and constructs the predetermined structure layer-by-layer aided by software. EBAM can be divided into selective electron beam melting (SEBM) and electron beam freeform fabrication (EBF^3) [55].

The forming process of SEBM is basically similar to that of SLM as shown in Fig. 7 [56]. To eliminate contamination from oxygen and other gases, SEBM must be conducted in a vacuum [57]. During the SEBM process, there is almost no reflection of the electron beam from the metal powders, and so energy utilization is higher than that in LAM, resulting in higher forming efficiency and recycling of un-used powders around the parts. However, the powder blowing phenomenon in which the pre-positioned metal powders are subjected to the impact of the electron beam and abrasion can affect the forming accuracy, leading to formation of pores and defects and possible failure of the forming process [57]. Moreover, owing to rapid melting and cooling by the high-energy electron beam, solidification shrinkage stress and structural stress may be introduced giving rise to deformation and cracking. In addition, since Mg powders are susceptible to burn-out and oxidation if the heat input from the electron beam is too high, production of Mg-based products by SEBM need further exploration.

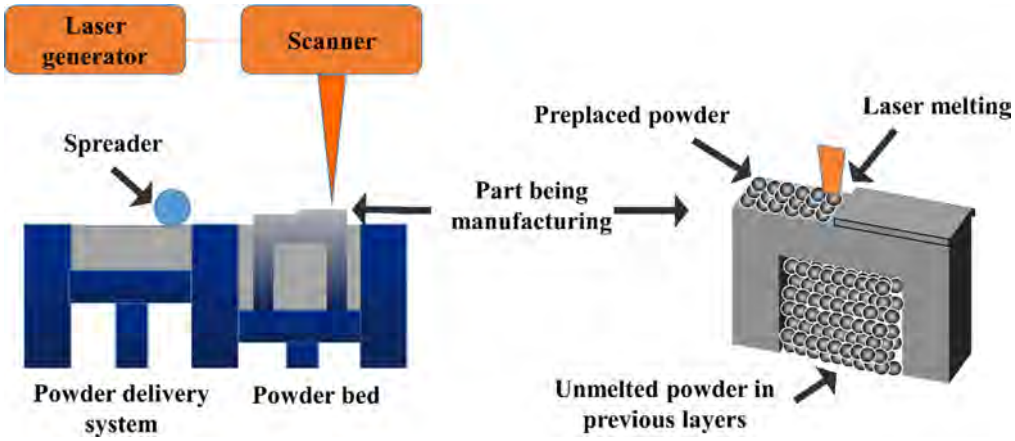

Fig. 6. Schematic of the SLM system [48].

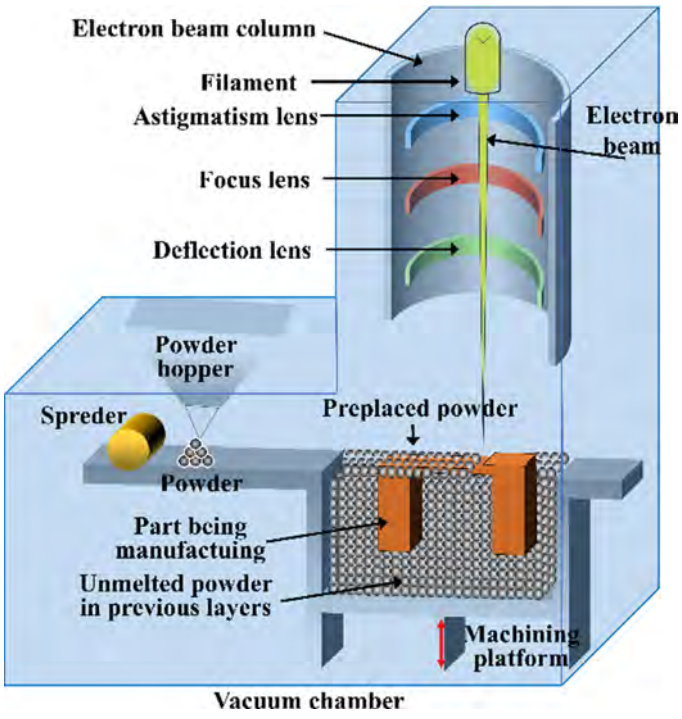

Fig. 7. Schematic diagram of SEBM [56].

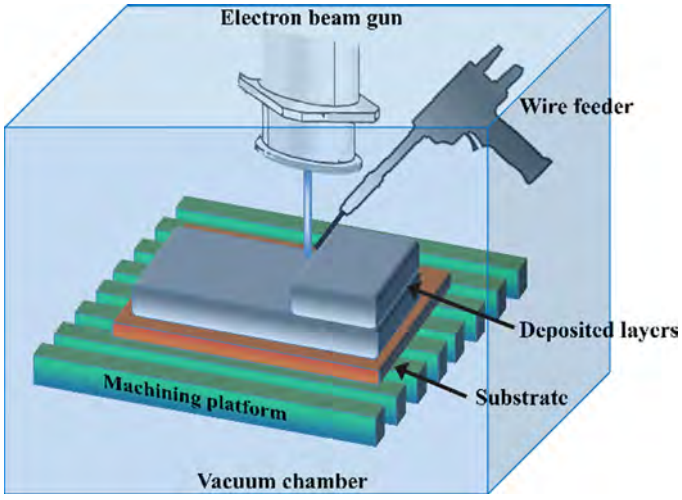

Fig. 8. Schematic diagram of EBF^3 [58].

Metal wires are the usual raw materials in EBF^3. As shown in Fig. 8 [58], the metal surface is melted by the electron beam in an inert environment followed by rapid solidification of the wire. The process proceeds layer-by-layer until the entire component is produced [59]. EBF^3 has high laser power and fused wire deposition efficiency and generally produces nearly formed parts but requires further machining. The additive process is carried out in an inert environment thus preventing air and other contamination to improve the quality [60].

Luo [61] have studied the effects of droplet transition on the forming of workpieces in EBF^3 and combined with the results obtained by Zhao et al. [62], a droplet transition height greater than 10 mm is shown to produce poor component appearance and instability in the additive process, as the recoil pressure of the vapor generated during metal melting affects droplet transition and stability of the welded joints. Zhang et al. [63] have used EBF^3 to prepare single-pass and multi-pass AZ31 Mg alloys with a high density (up to 99.2%) and changed the heat input by controlling the beam size and wire feeding speed in order to study the influence on the formation of the printing parts. In the range of 18∼30 mA, a larger beam current results in the larger relative burn loss of Mg and the larger proportion of Al, the larger is the grain size. In the range of 1.75∼2.50 m/min, the higher the wire feeding speed, the finer is the microstructure of the printed part and the closer the chemical composition to the original wire materials.

EBAM requires special vacuum and preheating equipment which is costly and limits the product size. EBAM is mainly used for high-strength steels, high-temperature alloys, and titanium alloys. The main research direction is to improve the precision, control the internal porosity, and solve the problem that the substrate blocks heat build-up with increasing printed layers, leading to increased element diffusion in the melted pool and melt pool instability during subsequent printing. As for Mg-based materials, development of EBAM is still in the infancy stage and there are insufficient practical experience and theoretical investigation.

3.3. Wire and arc additive manufacturing (WAAM)

WAAM is a rapid AM technique using an electric arc generated by welding techniques such as gas metal arc welding (GMAW) and gas tungsten arc welding (GTAW) as the energy source in conjunction with layer manufacturing in which a wire is fed through a wire feeding system for layer stacking [64,65]. The schematic illustration of GMAW-WAAM [66] is shown in Fig. 9. Welding grade argon (99.995% pure) is the shielding gas and the robot offers accurate motion for the welding torch to fabricate the components [66]. WAAM boasts high deposition efficiency and by using wires as the raw materials, eliminates the need to recycle the powders at the periphery of the parts to improve the safety. WAAM is the preferred method to prepare metallurgically bonded materials with a uniform composition, dense structure, high strength, and good toughness compared to the traditional castings and forgings [67,68]. Relative to other forming processes, WAAM has advantages such as the low cost, high efficiency, and fast near net forming of large and complex components [68].

GMAW is a welding method that uses a metal wire as the filler metal to form a welded joint in an inert gas such as argon or carbon dioxide. The arc between the wire and weld is the heating source and the wire carries a high welding current to transfer the molten wire droplets into the molten pool for rapid forming [69,70]. GTAW is also a welding process in which an arc is generated between the tungsten electrode or other non-melting electrode and base materials in an inert gas to melt the wire and form a welded joint. GTAW uses tungsten as the electrode and the high current may cause the tungsten electrode to burn, so that the forming efficiency is

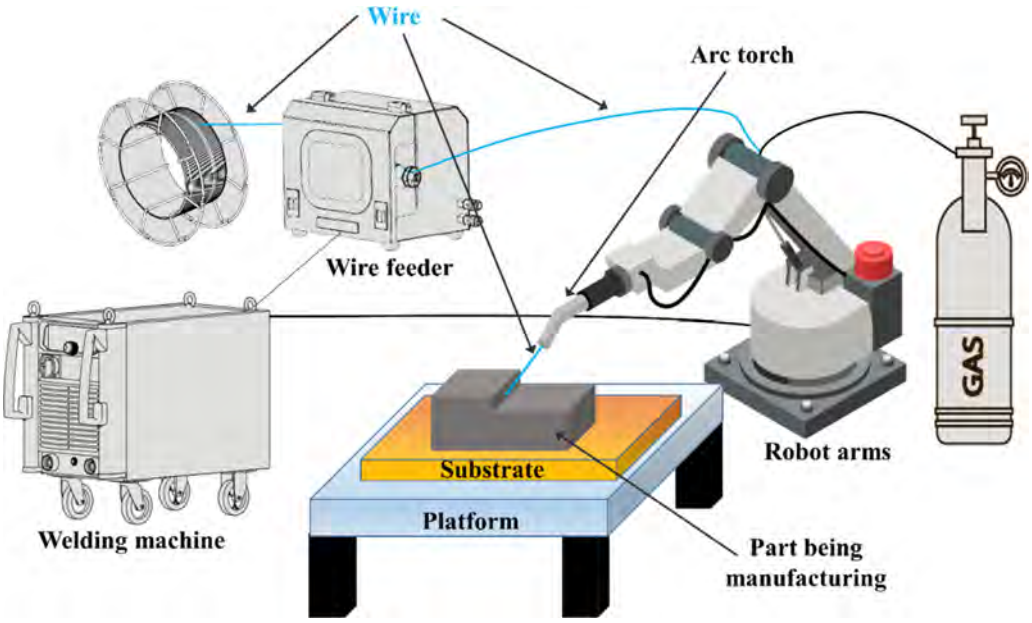

Fig. 9. Schematic diagram of GMAW-WAAM.

lower than that of GMAW. However, the arc generated during GTAW is more stable and there is generally no spattering of the melt droplets [71]. Therefore, GTAW-WAAM offers higher surface accuracy and forming quality, while GMAW-WAAM offers higher forming efficiency [71,72].

The study of AZ31 and AZ91 Mg alloys fabricated by WAAM demonstrates that reducing the heat input per unit length of the weld path without affecting the predetermined wire formability parameters allows grain refinement, improves the mechanical properties, and optimizes the forming accuracy [73–75]. Guo et al. [76] have studied the effects of different pulse frequencies (1, 2, 5, 10, 100, and 500 Hz) on the macroscopic morphology, microstructure, and tensile properties of the AZ31 Mg alloy and the results show that the pulsing frequency changes the molten pool oscillation, cooling rate, grain size, grain shape, and tensile properties. Yang et al. [77] have fabricated the AZ31 alloy with thin-wall components by WAAM by cold metal transfer (CMT). In the CMT-WAAM process, the CMT characteristics are chosen to deposit a wide and shallow weld bead with good wettability and low equivalent heat input. Compared to the conventional cast Mg alloy, the components prepared by CMT-WAAM have better mechanical properties [77,78]. Li et al. [66] have applied WAAM to prepare the single AZ31 membrane and the WAAM AZ31 exhibits distinct grain refinement with similar phase composition as the as-cast AZ31. The corrosion properties of the WAAM AZ31 and as-cast AZ31 are characterized by intergranular corrosion and micro galvanic corrosion, respectively.

In addition to the two main WAAM techniques mentioned above, plasma arc additive manufacturing (PAAM) has also been investigated [79]. PAAM with a higher arc compression, higher current density, and smaller heat affected zone is currently being used for AM of relatively small parts [80]. Since the principles and applications of PAAM are similar to those of these two processes, they are not described in this paper.

3.4. Solid-state additive manufacturing (SSAM)

SSAM is a new AM method based on friction stir welding (FSW) [81]. The friction heat between the hard metal head and workpiece and stirring action of the hard metal head introduce violent plastic deformation and the materials are thermo-plasticized as a result of hard metal head stirring and top forging. The schematic diagram of three SSAM processes are displayed in Fig. 10. Compared to traditional melt AM, FSW-SSAM involves no actual melting and solidification of the materials thus reduces the heat input to the part and eliminates metallurgical defects such as thermal cracks and residual stress. The grains in the materials are broken and refined by the action of the hard-metal head and the forming process does not require vacuum or inert gases [81,82]. These are major advantages for AM of large parts made of light alloys such as Mg and Al alloys.

Palanivel et al. [84] have prepared a multilayered stack of WE43 alloy using FSW-SSAM using different welding parameters and observed the grain orientation at the binding interface by electron backscattered diffraction. Defect formation is sensitive to the heat input and dynamic recrystallization under fragmentation of the stirring head leads to a finer grain size (2∼3 μm) and superior mechanical properties (tensile strength: 400 MPa and ductility: 17%). The maximum hardness of 115 HV is obtained in the as-fabricated state. Wlodarsk et al. [85] have reported that the Mg alloy components manufactured by FSW-SSAM can lose some strength (tensile strength decreasing from 298 MPa to 117 MPa) compared to rolled sheets due to the heat introduced by the additive cladding process that reduces cold-working strengthening. No

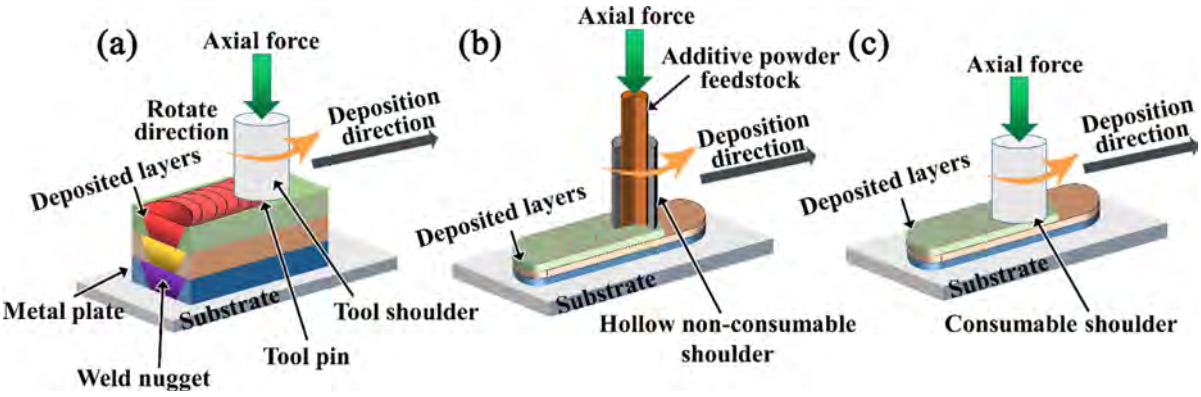

Fig. 10. Schematic diagram of three kinds of SSAM: (a) Friction stir AM (FSAM), (b) Additive friction stir deposition (AFSD), and (c) Friction surfacing deposition AM (FSD-AM) [83].

welding defects are found from the fracture interface and the mode is ductile fracture similar to that of the deformed AZ31 Mg alloy [86,87] caused by repeated stirring. The average grain size of each layer (4.5∼7.8 μm) is less than that of the initial AZ31 (8.5 μm). Ho et al. [88,89] have fabricated Mg-hydroxyapatite (HA) composites by FSW-SSAM and studied the effects of HA contents (5, 10, and 20 wt%) into AZ31 on the corrosion behavior and biocompatibility. The HA particles in the Mg-HA composites have the micro/nanometer scales after the friction stir treatment and the larger HA concentration improves the wettability and biocompatibility of the composites and refines the grains. However, owing to localized micro/nano-galvanic couples, incremental addition of HA has opposite effects on corrosion and the Mg-5 wt% HA composite has the best corrosion resistance.

4. Properties and applications of AM Mg-based biodegradable implants

4.1. Brief history of biodegradable Mg implants

The first surgical implants manufactured by AM are artificial acetabular cups, interbody fusion cages, skulls, clavicles, pelvis, dental implants, and orthopedic prostheses made of titanium and its alloys. In 2007, the first titanium alloy Delta-TT acetabular cup produced by electron beam powder 3D printing was implanted into a patient. So far, there have been more than 100,000 acetabular cups produced by AM worldwide [90]. Many studies and clinical applications are related to powder AM of titanium and its alloy, porous tantalum, titanium-nickel, cobalt-chrome, stainless steels, and other medical metals.

Similar to titanium, Mg has a low density, high specific strength, low modulus of elasticity, and good biocompatibility in addition to the unique biodegradability. Mg and its alloys have been studied as orthopedic materials for more than 100 years. In 2005, Witte et al. used Mg alloys in bone repair and found that the amount of new bone tissues was more than those around polylactic acid parts indicating higher osteoinductivity of Mg [91]. In 2013, the first Mg-Y-RE-Zr hollow bone screw (Magnezix®) developed in Germany received the CE product certification [92]. The Korea Food and Drug Administration (KFDA) has approved the Mg-Zn-Ca alloy screw (K-MET) for internal fixation of metacarpal fractures [93]. In 2016, Biotronik developed the first CE-marked Mg-alloyed intracoronary stent (Magmaris®) [94]. The Mg-Nd-Mn21 Mg alloy balloon-expandable biliary stent, Mg alloy vascular closure clip, and high-purity Mg oral shielding film or GBR have received CE certification. In 2020, Dongguan Eontec Co., Ltd. in China obtained CE approval for high-purity (99.99 wt%) Mg bone plates. The representative Mg-based products are described in Fig. 11.

Since 2010, a series of Mg-based biodegradable metal bone tissue engineering porous scaffolds and vascular scaffolds have been prepared by AM. Ng et al. [95] have adopted the SLM technology to fabricate pure Mg scaffolds in a protective atmosphere and revealed that it is a promising technique to fabricate Mg substitutes for orthopedic applications. Jauer et al. [96] have prepared AZ91 Mg alloy porous scaffolds using laser powder additive technology and confirmed that it is feasible to prepare porous biodegradable Mg alloy implants with a complex shape by SLM. WE43 Mg alloy porous mandibular prostheses have been produced by SLM based on CT scanning of the patient's jaw and the mechanical properties, *in vitro* degradation behavior, and biocompatibility of the AM WE43 Mg alloy porous scaffold have been assessed [97]. The porous 3D-printed Mg-Nd-Zn-Zr implant prepared by SLM exhibits excellent cytocompatibility, osteoinductivity, and antibacterial activity [98]. Although LAM of Mg surgical implants still poses risks of safety and quality, exploration is on-going and new advances are being made.

4.2. Properties of AM biodegradable Mg products

4.2.1. Microstructure and mechanical properties of AM biodegradable Mg products

The Mg alloy products prepared by powder or wire printing methods often contain dendrites and equiaxial crystals. It is generally accepted that the mechanical properties of equiaxed crystals are better than those of columnar crystals

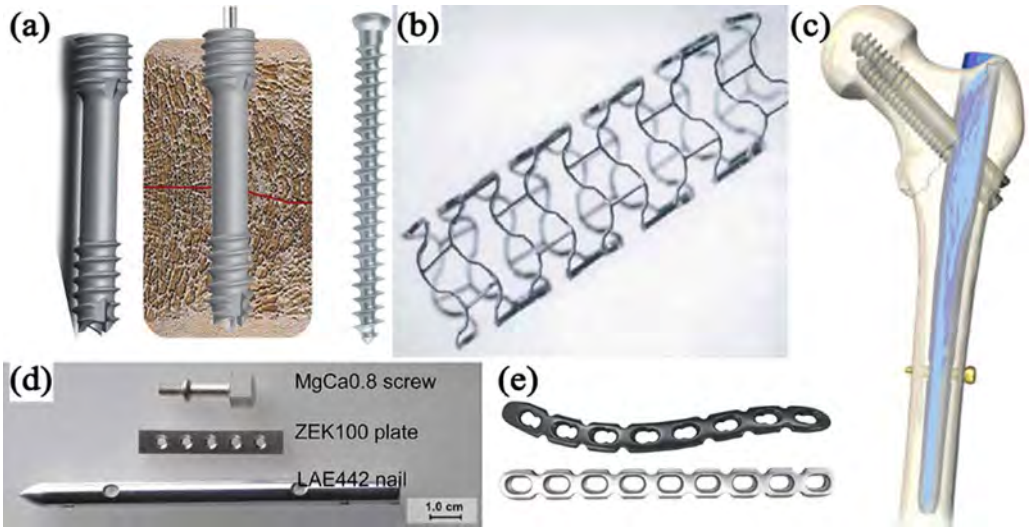

Fig. 11. Common Mg-based metal medical devices.

or dendrite crystals and hence, it is desirable to obtain small equiaxed crystals by metal solidification while reducing the percentage of columnar crystals/dendrite crystals as much as possible. Thermal-induced microcracks often exist in the microstructures of Mg-based AM products. This is due to the specific loss of heat flow direction in the printing process, supercooled and columnar dendrites at the solid-liquid interface, as well as volume shrinkage and heat shrinkage forming microcracks along the dendrite boundaries. However, the equiaxed crystal can undergo grain rotation and deformation to absorb strain and inhibit microcracks [99]. Therefore, the formation of equiaxed microstructures is of great significance in order to optimize the microstructures and mechanical properties of AM-Mg-based products. In addition, research on the laser powder printed MgZn alloy show that a higher zinc concentration has an adverse effect on densification of the alloy and the deposited layer produces solidification cracks and microcracks when the concentration exceeds 1 wt% [100].

Compared to traditional casting processes, the cooling rate in laser powder printing is faster, resulting in finer grain size and better mechanical strength of the formed specimens. Additionally, due to the maximum thermal gradient in the direction perpendicular to the substrate, the specimen's microstructure also exhibit anisotropy [26,101–103]. The preferred growth direction of the Mg-based metal powder with a close-packed hexagonal crystal is $<10\bar{1}0>$ in laser printing and there is an increased mechanical strength in the forming direction [104]. As shown in Table 1, power-based additive-manufactured bulk Mg alloys have higher hardness and ultimate tensile strength (UTS) than those prepared by the conventional process but they have lower elongations than those of the rolled and extruded ones [105]. The improved mechanical strength can be attributed to the high compactness and refined grains in the laser powder printed specimens and can be explained by the classic Hall-Petch relationship [105,106].

The microstructures of wire-based AM products are affected by the processing conditions. Both columnar and equiaxed grains are observed and the grain sizes are slightly larger than those of the powder-based AM products [46]. Table 2 shows the mechanical properties of Mg-based products fabricated by WAAM, indicating that Mg alloys fabricated by this method exhibit significantly higher ductility than those fabricated by powder-based AM methods. For instance, SLM-AZ91 has a total elongation of less than 2% (as shown in Table 2), whereas WAAM-AZ91 has a total elongation of 16% [116].

4.2.2. Degradation properties of AM biomedical Mg products

The degradable metal orthopedic implants or devices need to maintain the mechanical properties for 12∼24 weeks depending on clinical requirements [118]. For bone plates and screws, a corrosion rate of less than 0.5 mm/y is usually required. With regard to biodegradable metal materials such as dense Mg, addition of alloying elements usually reduces the grain size and the fine-grained microstructure may reduce the corrosion rate [105] which is also related to the passivation properties of the surface [119]. Galvanic corrosion between the precipitated second phase and matrix also affects the corrosion rate of AM degradable metals [120,121].

In vitro investigations of SLM porous Mg show that the corrosion properties are related to the location. After immersion in revised simulated body fluid (r-SBF) for 4 weeks, the center of the porous WE43 scaffold with a diamond structure degrades faster than the edge. However, the degradation behavior of porous pure iron scaffolds under the same conditions is opposite [122]. The weight losses of porous WE43 Mg alloy and porous pure zinc prepared by SLM after immersion in simulated body fluids for 28 days are 20% and 8%, respectively, which are consistent with the bulk degradable metals produced by traditional smelting methods [123–125]

Shuai et al. [126] have prepared hydroxyapatite (HA)-reinforced MgZn composites by SLM and the grain size of the products decreases continuously with HA contents attributable to heterogeneous nucleation and more nucleation during solidification. The degradation rate in SBF is slowed due to the

Table 1
Mechanical properties of common Mg alloy products prepared by SLM.

Composition	Yield strength (MPa)	UTS (MPa)	Elastic modulus (GPa)	Hardness (HV)	Elongation (%)	Ref.
Pure-Mg	/	/	27∼33	60∼95	/	[107]
AZ91D	253	/	/	90∼108	2	[108]
AZ91	274	296	/	85	1.2	[109]
	237	254	/	100	1.8	
AZ91	308	345	/	/	1	[110]
	219	273	/	/	3.3	
AZ61	233	287	/	/	3.1	[111]
	225	261	/	/	2.8	
	216	239	/	/	2.1	
ZK60	132	/	/	81	/	
ZK60-0.2Cu	144	/	/	88	/	
ZK60-0.4Cu	158	/	/	95	/	[112]
ZK60-0.6Cu	155	/	/	101	/	
ZK60-0.8Cu	148	/	/	105	/	
Mg-1Zn	148	/	/	50	11	
Mg-2Zn	71	/	/	46	2.5	
Mg-4Zn	60	/	/	58	2.8	
Mg-6Zn	45	/	/	65	1.5	[100]
Mg-8Zn	44	/	/	78	2.1	
Mg-10Zn	63	/	/	76	2.2	
Mg-12Zn	74	/	/	80	3.3	
Mg-1Sn	/	60	/	49	/	
Mg-3Sn	/	75	/	53	/	[113]
Mg-5Sn	/	80	/	62	/	
Mg-7Sn	/	75	/	65	/	
WE43	296	308	/	/	12.2	[26]
Mg-Gd-Zr	180	228	/	80	2.2	[114]
Porous-JDBM	/	4.07∼16.25	0.2∼0.76	/	/	[24]
Porous-WE43	/	12.5∼31	/	/	/	[115]
Porous-WE43	/	/	0.7∼0.8	/	/	[97]

Table 2
Mechanical properties of typical Mg-based materials prepared by WAAM.

Composition	Yield strength (MPa)	UTS (MPa)	Elongation (%)	Refs.
AZ31B	143 (Transverse)	183 (Transverse)	5.5 (Transverse)	[74]
	160 (Transverse)	196 (Transverse)	6.0 (Transverse)	
	163 (Transverse)	201(Transverse)	6.8 (Transverse)	
	165 (Transverse)	214 (Transverse)	7.2 (Transverse)	
	189 (Transverse)	193 (Transverse)	4.5 (Transverse)	
AZ31	104	263	23	[76]
AZ31	71 (Transverse)	210 (Transverse)	7.6 (Transverse)	[77]
	132 (Vertical)	150 (Vertical)	10.6 (Vertical)	
AZ31	85 (Transverse)	225 (Transverse)		[78]
	126 (Vertical)	211 (Vertical)		
AZ80M	150 (Transverse)	310 (Transverse)	15.4 (Transverse)	[117]
	120 (Vertical)	240 (Vertical)	12.2 (Vertical)	
AZ91		245	16	[116]

reduced grain size and formation of a protective bone-like apatite layer. Hence, bioceramic materials incorporated into Mg-based alloys by AM can retard the degradation rates, although there have been limited reports on AM of Mg-based metal bioceramic composites and the corresponding degradation properties.

4.2.3. Biocompatibility of AM biodegradable Mg products

As AM Mg-based products are among the most promising biodegradable implant materials, their biocompatibility is a critical issue. Nonetheless, there have been few results related to the *in vitro* and *in vivo* biocompatibility of AM porous biodegradable Mg implants and evaluation of biocompatibility is mostly *in vitro* [90]. The factors affecting the biocompatibility of degradable metals are the chemical composition and degradation products. Therefore, it is essential to study the interaction and impact of these degradation products and their metabolic products on tissues to guide the design and development of Mg-based orthopedic repair products [127]. In the future, the material composition design of raw materials (whether powders or wires) for 3D printing of biodegradable Mg must adhere to the fundamental principles of biocompatibility and biodegradability requirements for design and application. The grain structure of AM bulk biodegradable metal

materials is finer and may have texture compared to those of traditional materials. The influence of these factors on the biocompatibility of the materials is currently under research and evaluation, and no definitive conclusion has been reached yet. However, when compared to bulk biodegradable metal products manufactured by traditional processes, AM products should exhibit similar macroscopic cell biocompatibility [105,128,129].

The advantages of AM porous biodegradable metal implants are that the three-dimensional pores can provide channels for nutrient transportation and metabolite excretion to facilitate ingrowth of new bone tissues [130,131]. The geometry and microstructure of porous materials are different from those of conventional bulk materials, leading to different biodegradation properties and cell response. The biocompatibility of scaffolds can be improved by modulating the porous structure of scaffolds [132] and scaffolds with a diamond structure have comparable mechanical properties as trabecular bones even after immersion in SBF for 4 weeks. The volume loss after soaking for 4 weeks is about 20% and the *in vitro* cytotoxicity to MG63 cells is less than 25% [97].

The surface morphology of AM products also affect the biological response [133]. A nanoscale surface topology induces osteogenic differentiation in mesenchymal stem cells (MSCs) and promotes adhesion of osteoblasts, and the rates of bone tissue generation increase with the curvature of the porous scaffolds. Adhesion is faster on the concave surface than convex and flat surfaces. This provides a promising design and research idea for future surface topographical design of AM degradable Mg biomedical devices [134–136].

4.3. Factors affecting the properties of AM Mg-based products

4.3.1. Raw materials

4.3.1.1. Spherical powders. The quality of medical devices depends on the physical and chemical properties of spherical metal powders [137]. Mg is reactive and reacts easily with oxygen, nitrogen, and other gaseous elements and the exothermic reaction between Mg powders and oxygen can be violent. Therefore, a large oxygen content in the Mg powders affects the AM process and the higher energy required to melt an oxide layer produces a higher melt pool temperature and increases evaporation of Mg powders spurring formation of defects such as balling,micropores and inclusions [88]. The size of the Mg powders also affects the quality of the 3D printed products. For the same energy input, the melt pool temperature is higher for pure Mg powders due to oxidation and spheroidization, and the relative density of the spherical Mg powders also varies depending on the size [138]. In addition, the amounts of alloying elements in the Mg powders impact the quality of the printed products [100].

Spherical metal powders for 3D printing must meet the requirements of high purity, good sphericity, small particle size and narrow distribution, high bulk density, no porosity, and good flowability and plasticity [137,139,140]. Guangzhou Sailong AM Co., Ltd. has produced high-quality WE43 Mg alloy spherical powders containing rare earth elements by plasma rotating electrode processing (PREP) with the chemical composition (wt%) of Y 4.01, Re 3.04, Zr 0.51, Fe 0.007, Cu 0.004, N 0.004, O 0.005, and Si 0.004 (Fig. 12).

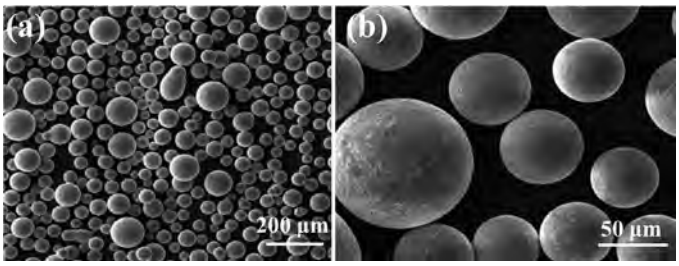

Fig. 12. WE43 Mg alloy spherical powders prepared by PREP.

4.3.1.2. Round wires. Mg has a lower melting point, boiling point, higher chemical activity, and thermal expansion coefficient, which not only increase the manufacturing cost and safety hazards, but also brings technical challenges for accurate forming and quality control of AM products. Therefore, with the advent of EBAM in 2002 [141] and subsequent development of WAAM, the metal wire printing technology has become increasingly popular on account of the low manufacturing cost, high deposition efficiency, and ability to produce larger products than powder 3D printing. As a result, there have been growing attention and research on the wire-fed AM technology, which has become an important direction for advanced manufacturing.

Initially, WAAM using metal wires as raw materials is mainly used for welding connections with repair of large-scale equipment. However, the heating source and metallurgical properties created by welding wire accumulation are quite different from those of WAAM of multi-layer and multi-pass accumulation, resulting in substandard metal composition, splashing, and slag inclusion in WAAM. Therefore, it is necessary to develop special Mg wire raw materials for WAAM with good chemical composition and stability.

4.3.2. AM processes

4.3.2.1. Powder printing. Mg powders with different compositions and AM products with complex geometry require high powder quality as well as printing processes and equipment. In addition to the chemical composition, the treatment process and morphological characteristics of the powders influence the AM process. Good fluidity and powder quality are vital to printing.

Compared to conventional manufacturing processes, powder printing has different features: (1) Evaporation of powders can change the specimen composition; (2) The fast cooling rate refines the grains and forms a non-equilibrium structure to reduce segregation and second phase precipitation; (3) The large temperature gradient stimulates grain-oriented growth to form a certain texture [142]. At present, the heating sources used in powder printing are mainly electron beams and lasers. EBAM can be applied to coarse powders (60∼100 μm),

whereas LAM powders are smaller (10∼60 μm). In LAM, the laser spot is smaller, heating is more accurate, cooling is faster, forming accuracy is higher, and the equipment and maintenance costs are lower. Furthermore, it does not require a vacuum like EBAM requiring only an inert gas for protection [104,143]. Owing to the high activity, flammability, and explosiveness of Mg powders, LAM is the primary method used in the research and development of Mg-based products both domestically and abroad.

Previous studies have confirmed that a number of processing parameters affect the laser powder printing process and product quality, among which the laser power and scanning rate have significant effects on the powder bed melting pool, evaporation, and deposition, which are reflected in the internal density and surface roughness of the products [139]. The density of 3D printed products is determined by the powder melting behavior caused by the interactions between the laser and powders and the quality of products with good density is quite good [105]. A high energy density can evaporate the powders causing local vapor pressure in the molten pool and splashing of the molten substance resulting in the formation of defects such as keyholes and low-density structures and changes in the chemical composition of the specimens and dimensions. On the other hand, a low energy density produces insufficient melting of powders. For example, Esmaily et al. [144] have found that a low energy input during the formation of WE43 alloy produces a large number of pores and un-melted powders, resulting in reduced density and mechanical strength. Therefore, an optimal balance must be struck in order to obtain the appropriate molten pool temperature and wettability to ensure good dimensional accuracy and high density of more than 98% [139]. Zhang et al. [145] have found that when the laser energy density is increased from 7.5 J·mm^{-3} to 15 J·mm^{-3}, the porosity of AZ91 decreases from 25.5% to 18% but when the laser energy density is increased from 15 J·mm^{-3} to 20 J·mm^{-3}, the porosity increases. It is notes that the interactions between Mg and the gases in the AM chamber causes oxidation and nitridation on the surface of the products. Therefore, to obtain uniform chemical composition and tissue properties, as well as high dimensional accuracy in the design of medical Mg-based medical devices, further research is needed to deepen the powder AM process.

4.3.2.2. Wire printing. Although LAM is mainly used in precision and rapid prototyping of complex parts, some metals have high laser reflectivity thus reducing the efficiency. In WAAM, the formation accuracy is difficult to control but in processing of large and complex components, it has the advantages of low cost, high efficiency, fast forming, and high deposition rate. However, the slower cooling rate and longer intergranular liquid phase filling time compared to LAM can reduce the tendency of thermally induced cracks in light metals such as Mg and Al [146].

At present, although WAAM using metal wires as the raw materials has process simplicity, high deposition rate, and energy utilization rate for Mg, there are still problems such as poor controllability and insufficient accuracy thus requiring subsequent mechanical processing. Processing control for WAAM determines the forming quality and efficiency of deposited metals. Nowadays, research of process control of WAAM involves three aspects, namely parameter control, real-time automation control, and path planning. The main parameters to control the process are the current, voltage, wire feeding rate, heat input, deposition rate, and interlayer temperature. The proper parameters are needed for good forming quality and minimal internal defects. Real-time automation control improves the forming accuracy and intelligence of WAAM. Path planning consists of the component slicing method, path filling method, and planning for each slice. In view of the shortcomings of low dimensional accuracy and large surface roughness of arc printing products, strict control of the arc welding power, droplet transition, wire feeding rate, and starting and stopping points of the arc are the key factors. Since the thermal diffusivity decreases with the accumulation layer, which leads to the accumulation of interlayer temperature. Hence, it is also necessary to consider the parameters of the printed wires, deposition process for different number of layers, and the optimization design of temperature control between each layer. The width of the cladding layer increases linearly with bead welding currents and decreases with scanning rates. The deposition height decreases with increasing scanning rates and the influence of the welding current is more complicated. In different path manufacturing processes, the parameters need to be adjusted to maintain dimensional accuracy of the products [147].

Compared to LAM and WAAM, EBAM has the characteristics of high energy density and high utilization rate [148]. An electron beam possesses strong penetration ability and deep melting pool and can re-melt additive manufactured parts to reduce interlayer unfusion and porous defects in AM. It has advantages in integrated rapid prototyping of large and complex structural parts of light metals and AM repair of high-precision damaged workpieces [141]. However, because Mg powders used in EBAM produce a large amount of smoke when melted by a high-energy electron beam, it is easy to pollute the vacuum environment and not suitable for processing of Mg metal products which normally use laser powder AM for processing [142]. Nevertheless, it has been demonstrated that non-vacuum electron beams are suitable for wire welding of Mg alloys such as wrought AZ31 Mg alloy, AM50A, and AZ91D cast Mg alloys. It is expected that non-vacuum electron beam wire printing boasting high speed, efficiency, and high automation will spur the development of large-scale production of AM Mg-based products in the future.

4.3.3. Heating systems

Since Mg powders are emitted violently by a high-energy laser beam, the metal vapor blocks and scatters the laser beam consequently affecting the forming quality and therefore, a gas circulation system is utilized to remove the metal vapor. In addition, real-time *in situ* monitoring of the molten pool and powder bed can be implemented to perform imaging and defect identification aided by machine learning. Meanwhile, the theoretical understanding of the forming process should be

enhanced so that the interactions between the heating source and powders, powder transfer and flow of the molten pool, temperature distribution of the molten pool, and cooling rate can be optimized to improve both the hardware and product quality [149,150].

WAAM has undergone rapid development in the past decade and is used in manufacturing high-performance metal components. However, owing to the complexity of WAAM, the equipment, process, and raw materials affect the forming quality and sustainability of the manufacturing process. Various WAAM systems have been developed to incorporate arc control (such as laser-constrained WAAM system), improve the forming efficiency (such as the WAAM equipment at Huazhong University of Science and Technology consisting of 5 arc guns), etc. Although WAAM can fabricate large components, because the arc is a flexible conductor, arc instability occurs due to external factors to degrade the forming quality due to formation of pores.

In order to improve the quality of AM products, novel systems and processes combining additive and subtractive manufacturing have been proposed to improve the dimensional precision and production efficiency. For example, since plastic processing after AM can eliminate defects in the components, an integrated heat source equipment system has been developed for WAAM [151]. By considering heat accumulation in WAAM, Lu et al. [152] have proposed the annealing after additive processing and timely subtractive cutting to reduce the large stress caused by repeated additive heating and subtractive cooling and shorten the cooling time. Additionally, the subtractive process can improve the metal cutting performance, refine the surface grains in the cutting layer, and protect the cutter bits from abrasion. With regard to the surface morphology, stress transmission and cutting mechanism of the components under residual heating after integrated additive and subtractive processing need to be studied thoroughly in the future [152,153].

4.3.4. Structural design

Common biomedical AM products can be divided into dense and porous ones according to the structure and functionality. In terms of the structure design, dense components are relatively simple and the dimensions and surface structure can often be improved by secondary machining, whereas porous products are difficult to modify by subsequent processing. Owing to dynamic degradation, the properties of porous products change with time and so materials and process design is more complicated. It is necessary to consider four aspects including *in vivo* degradation, mechanical properties, biological characteristics, as well as physiological functions. Before designing the porous structure, additional aging effects associated with degradation that compromise the mechanical integrity and cell growth must be assessed.

The desirable implant must have sufficient mechanical strength and be compatible with surrounding bone tissues, so that sufficient mechanical support and stress conduction are provided during healing [154]. According to the book “Basic Orthopedic Biomechanics and Mechano-Biology”, the basic mechanical properties of the hard femur and cortical bone in adults should have tensile strength of 51∼133 MPa, compressive strength of 133∼193 MPa, and elastic modulus of 11.5∼17.0 GPa [155]. Previous studies has shown that the yield strength of pure Mg dense blocks produced by AM is 51 MPa and the elastic modulus is between 27∼35 GPa, which are comparable to those of human cortical bone [156]. Wei et al. [109] has achieved yield strength of 254 MPa from AZ91D alloy produced by SLM by exploiting solid solution strengthening, grain refinement, and second phase strengthening. It is superior to human cortical bone and meets the design requirements for yield strength of degradable metal bone fixation devices [129]. The mechanical strength of the porous AM Mg-based specimens is inferior to that of the compact components, and it depends heavily on the structural design and porosity [24,115]. Porous 3D printing metal biomaterials mainly adopted structural design based on beams and sheets, while the units for degradable porous metals such as Mg include the diamond type, gyroid, and bone biomimetic structure (Fig. 13) in order to optimize the mechanical properties, degradation rates, and biocompatibility. Yuan et al. [24] have conducted a comparative analysis of the mechanical properties of three structural AM Mg alloy scaffolds mentioned above. The mechanical properties of 3-type scaffolds are in the range of the cancellous bone strength. Meanwhile, the scaffold with the biomimetic structure has relatively lower mechanical strength compared to the other two scaffolds due to the higher failure tendency of the partly thin strut. The pores can cause stress concentration thus compromising the mechanical properties of 3D-printed Mg alloys. Therefore, as the porosity increases, the mechanical properties of Mg alloys worsen [157]. Furthermore, the geometry affects the corrosion and fatigue behavior of porous AM Mg products [158].

Porous Mg-based bone repair materials have traditionally been prepared by powder metallurgy based on an internal porous design achieved by adding a biodegradable pore-forming agent (foaming agent) beforehand. With the advent of advanced AM technology, it is now more convenient to use this method to prepare Mg-based metal porous materials and Mg-based metal-bioceramic porous composite materials, with the internal porous structure pre-designed in one step by computer-aided design (CAD). Although powder AM can produce different types of porous Mg-based bone repair materials in one process, the CAD design for irregular three-dimensional connected pores is difficult, and the manufacturing process is complex, time-consuming, and inefficient as well. In this respect, our research team has designed Mg-based bioceramic bone repair materials with an internal three-dimensional porous structure by using Mg-based composite filaments containing the bioceramic and pore-forming agents [159]. This method has the advantages of being convenient, efficient, practical, and economical.

4.3.5. Post-treatment

The porosity and surface roughness of AM Mg products affect the mechanical properties, degradation rates, and biological interactions in the human body after implantation.

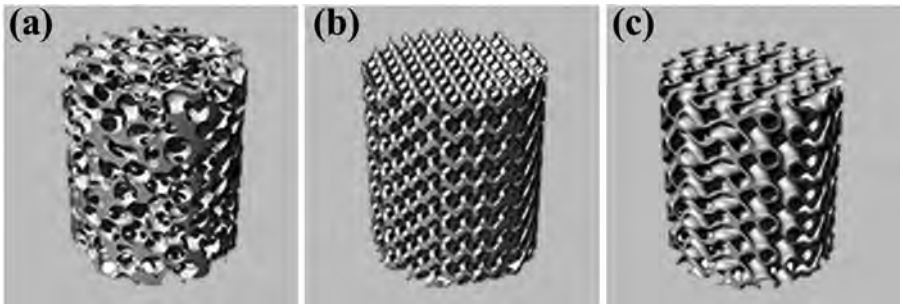

Fig. 13. CAD design models of three different scaffolds: (a) Biomimetic, (b) Diamond, and (c) Gyroid [24].

Table 3
Comparison of AM techniques for Mg-based materials.

Technology	SLM	EBF	WAAM/PAM	FSAM
Heat source	Laser	Electron beam	Arc/Plasma arc	Friction
Raw materials	Powder	Wire	Wire	Sheet/bar
Environment	Inert gas atmosphere	Vacuum	Inert gas/open	/
Dimensional precision	High	Low	Low	Medium
Forming efficiency	Low	High	High	Medium
Size limitation	Medium	Medium	Large	Large
Residual stress	High	Medium	High	Low
Post processing	Less	More	More	More

The surface of LAM Mg products contains residual particles which not only increase the risk of bacterial colonization, but also adversely affect the biocompatibility [160]. For degradable porous components, the common sand blasting and chemical erosion treatments cannot produce uniform and smooth surfaces and the inhomogeneity may produce different degradation behavior at different locations of the products and cause premature loss of mechanical integrity [123,125]. In addition, the residual stress caused by sand blasting may affect degradation as well.

Heat treatment, hot isostatic pressing (HIP), and surface modification are usually used to improve the properties of AM products. To maximize the benefits of Mg-based products by WAAM, Guo et al. have investigated the effects of different heat treatment procedures on the microstructures and mechanical properties of the WAAM AZ80M alloy. Alloying micro-segregation is improved as the eutectic structure dissolves, but although the strength and ductility can be improved by the hot treatment, the micropores in the interlayer region restrict the improvement of the mechanical properties [161]. After HIP treatment of the WE43 Mg alloy by SLM, HIP was demonstrated to be an effective mean to eliminate defects and obtain samples with high densification [144]. HIP can densify SLM WE43 Mg alloys with high porosity but cannot improve densification of products with smaller porosity [25]. The cooling rate of SLM is significantly higher than that of the traditional cast, but the rapid cooling rate is not conducive to precipitation of the strengthening phase. Moreover, the residual stress, texture, and mechanical anisotropy caused by fast cooling rate can also be eliminated by post-heat treatments [162]. Alexander et al. have reported that the surface of porous WE43 Mg alloy scaffolds produced by SLM can be post-treated by plasma electrolytic oxidation that can mitigate degradation during early immersion in SBF. However, the influence of the coating on the biocompatibility of the SLM WE43 has not been studied [115]. In summary, although researchers have employed different post-processing methods to improve the performance of 3D printed Mg-based products, more studies are necessary to determine the surface characteristics and overall functionality of porous Mg-based products by AM.

4.4. Development and applications of new AM biodegradable Mg products

As an advanced rapid prototyping technology developed in the late 1980s, AM can realize rapid manufacturing of products without molds and provide a feasible way for efficient preparation of high-performance products with a complex structure. It has been widely used in the aerospace, marine, biomedical, and rail transportation industries. By using Mg powders or wires as raw materials and choosing laser, electron beam, and arc as the heating mechanism, different AM protocols have their own advantages and disadvantages as shown in Table 3. In practice, the most economical and straightforward methods that can satisfy the requirements should be adopted.

Because of the good dimensional precision and non-dense characteristics of the products, LAM is currently being developed for small and precise surgical implants such as orthopedic and dental implants as well as other medical precision structural components. The development of LAM for biomedical Mg-based products has mostly focused on improving the density to obtain better mechanical properties. In recent years, the clinical application of porous degradable Mg-based surgical implants in the fields of orthopedic repair and

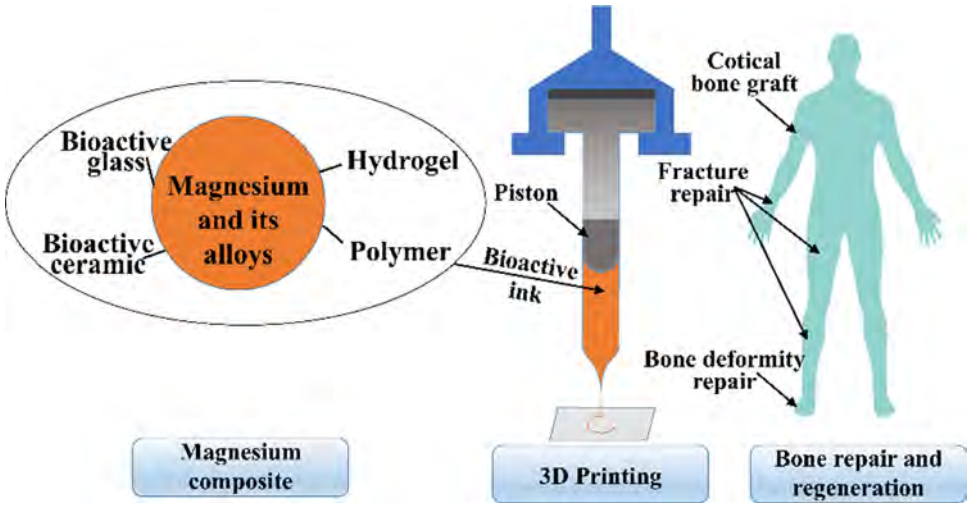

Fig. 14. “Ink” 3D printing of Mg-based composites.

tissue engineering has been increasing, and how to achieve reasonable material selection and optimize AM processes to meet the high demand requires further exploration [163,164]. Traffic-related injuries, sports injuries, and bone tumors result in bone defects with various size and shape. Although traditional bone cement and porous ceramic fillers have certain therapeutic effects in the treatment of large bone defects, bone cement can produce complications such as high pressure in the bone marrow cavity after curing. It is not degradable and ceramic bone restorative fillers are easy to break. Therefore, the development of personalized Mg-based bio-ceramic porous bone repair materials is expected to be the focus of future research. Besides improving the strength and toughness of bone prostheses, the weak alkaline environment formed by the degradation of Mg can improve the osteogenic effects of the defect sites. Furthermore, internal three-dimensional perforated structures are conducive to bone growth.

Since the role of many surgical implants is temporary *in vivo*, Mg-based materials with biodegradable properties will continue to be developed to cater to different medical applications. AM of Mg-based composites containing active ingredients such as poly (L-lactic acid) (PLLA), poly (lactic-co-glycolic acid) (PLGA), hydroxyapatite (HA), β-tricalcium phosphate (β-TCP), hydrogels, bioactive ceramics, and bioactive glass is becoming an emerging research area (Fig. 14), because they can better adapt to human cancellous bones. Therefore, the use of porous bone repair scaffolds will continue to expand in the future.

With the advent of AM, it is more convenient to prepare Mg porous materials and Mg-based metal bio-ceramic porous composite materials with predesigned internal porous structures. The authors have designed Mg-based bio-ceramic bone-repair implants with a three-dimensional through-hole porous structure with self-made Mg-based composite powder core wires containing bio-ceramics (HA, β-TCP, etc.) and a pore-forming agent ($MgCO_3$, NH_4HCO_3, etc.) for bone restorative billets with different shape by WAAMZL. The internal porosity of the billet is controlled by the subsequent sintering pore-forming process, so that the degradable metal-based bioceramic porous bone restoration devices can be prepared quickly, efficiently, and at a low cost.

5. Development trend and prospective of AM biomedical Mg

Mg and Mg alloys are advanced structural and functional materials with excellent attributes such as the light weight, non-magnetic properties, high specific strength and stiffness, good biosafety, as well as biodegradability *in vivo*, rendering them suitable for surgical implants and orthopedic devices. China has the world’s largest reserve of Mg and strong production capacities. On the heels of the rapid development and widespread application of AM technology in the military and civilian fields, AM of Mg-based materials has garnered increasing attention and is expected to become a new high-tech industry due to the high efficiency, added value, and sustainability. The prospects for the development of biomedical Mg-based AM technology are broad, and future research and development trends and prospects are discussed from the following different perspectives.

5.1. Standardization of raw materials and consumable items with high quality and low cost

The quality of AM products depends on the chemical composition, morphology, as well as physical and chemical properties of the raw materials. The manufacturing process also impacts the strength, modulus, and elasticity of the products [46]. Due to the high activity of Mg, it oxidizes and evaporates easily especially at a high temperature. A high-temperature heating source can cause large deviations in the chemical composition of the printed parts and original powder. In addition, owing to repeated melting and rapid solidification of the powder and other physical metallurgical processes, the printed products have different microstructure and mechanical properties compared to those produced by con-

ventional manufacturing [165]. Therefore, the development of special consumables for AM such as high-quality spherical powders is crucial.

The development and production history of Mg-based metal spherical powders for 3D printing is relatively short, especially in China, and only a few professional enterprises can pass the quality verification for commercial Mg powders. The commercialization and standardization of Mg powders raw materials have become critical factors limiting the research and application of AM. On the heels of continuous advance of electron beam, arc, and plasma AM technologies, the demand for AM products for better quality and lower cost is increasing. Compared to Mg powders, Mg wires have advantages such as a short processing cycle, simple and green process, as well as chemical composition-microstructure-mechanical properties that are easy to regulate at a low cost [78]. Hence, wire AM technology is attracting more attention. With the emergence of various new materials such as nanomaterials, bioglass, polymers, and Mg matrix composite materials, the development of special Mg-based composite wires that meet the requirements of 3D printing, as well as the establishment of standardized production and testing technical specifications, have high scientific significance and economic value, thus spurring the study and development of high-performance, multifunctional (antibacterial, bone-promoting, etc.), composite, porous, and cost-effective new Mg-based biomedical devices.

With the continuous development and increasing clinical demand for biomedical Mg 3D printing products in the field of personalized and precision therapy, the traditional production mode of mainly metallurgical production and material subtractive processing is expected to be replaced partially by the wire fusion AM technology [26], because its development will effectively promote green and low-energy consumption together with a short production cycle [166]. It is expected to become another area of technological innovation besides powder printing. Therefore, increasing research and investment in high-quality consumable products such as spherical powders and round wires for 3D printing is of great significance.

5.2. Integration and intelligent development of special equipment for AM of Mg biodegradable metals

The AM forming process of Mg-based materials still has technical problems such as inconsistent product composition, poor controllability, lack of precisely formed products, and need for secondary processing, the future AM frontier of biomedical Mg-based metals should focus on the “multi-energy fields, multi-materials, high efficiency, high precision, high performance, and large size range” [167]. Specifically, according to the characteristics of the powder and wire consumables and the product shape and performance requirements, a variety of heating sources such as “laser-arc hybrid AM” combining the high deposition rate of arc heat source and the dimensional accuracy of laser heating sources have been studied [168,169], or based on the arc AM equipment containing industrial robots and arc heating sources, composite embedded laser systems, multi-signal sensing and monitoring devices, as well as process database and machine learning systems can learn from each other to complement each other’s strengths to improve the integration and intelligence level of AM of Mg-based metal materials [170,171]. Although there have been some researches and innovations on the dimensional accuracy of small thin-walled, cylindrical and other simple structural parts made of arc fused AM Mg [156], there are still many challenges in improving the dimensional accuracy of large complex structural parts as well as chemical composition and defect control of products containing gradient materials and composites. On the one hand, the R&D of multi-channel wire feeding, wire-powder mixing technology, and supporting composite printing process is required [172], and on the other hand, the method and process of additive and subtraction composite manufacturing should be investigated in-depth. Auxiliary optimization schemes such as secondary plastic processing and heat treatment should also be explored [160]. After the process is mature and stable, an integrated, intelligent, and continuous operation equipment with arc AM as the core should be developed.

5.3. Exploration and innovation of proprietary AM technology for biodegradable Mg products

Compared to other bioinert metals such as titanium alloys, AM of degradable Mg materials is more complex [24]. If the AM process is not proper, the mechanical properties and degradation behaviors will be compromised. AM of Mg-based materials is mainly based on layer-by-layer laser melting of powder materials involving metallurgical processes such as material melting, evaporation, solidification, and solid phase transformation, which inevitably cause drastic changes in the materials composition, microstructure, and properties [54,166]. The AM process is not suitable for mixed different materials and the technological innovation of composite materials and products with gradient structures is limited. Therefore, it is necessary to develop more advanced AM technology with high reliability, high precision, high flexibility, and low cost. Firstly, based on the advantages of laser powder AM in processing of dense parts with relatively mature precision and compactness control, the processing parameters such as the laser beam density and scanning rate as well as chemical composition, microstructure, and mechanical properties of the printed products require personalization, miniaturization, precision, and low cost [46]. In addition to Mg vascular stents, Mg-based surgical implants with porous structures and degradability are expected to spur development of the orthopedic market [130]. In order to attain satisfactory compression and moderate degradation, powder AM technology still faces many challenges in terms of the processing parameters, chemical composition, porous structure, microstructure, and mechanical properties [24]. Secondly, in view of the processing characteristics that arc fuse wire AM can produce large and complex products, the appropriate slicing methods and in-slice path planning strategies can be formulated to prepare

different structural products and specific wire materials. A database can be formed and automatic software can be designed based on the database [173]. The process can be optimized continuously in real time by controlling the droplet transition, temperature distribution, molten pool morphology, heat dissipation, and other actual conditions in the AM process. Subsequently, based on a large number of experiments and experiences, the correlation model of process parameters and forming size can be established for reference [174,175]. Computer software should be used to simulate and predict the manufacturing process and a dynamic response mechanism of "material property-manufacturing process-microstructure-mechanical properties" can be established to improve the accuracy and efficiency of the products. Finally, development of high-quality and defect-free 3D printing products are required and exploring the superposition and complementarity of non-vacuum electron beam and arc fuse printing is conducive to the development of Mg AM products [176].

5.4. Structural optimization of the design and efficacy of AM biodegradable Mg-based products

The major advantages of AM are the high efficiency and precision for products with individualized and complex geometric structures, especially orthopedic surgical implants such as acetabular cups and bone defect repair patches with three-dimensional porous structures. However, the current design principles and methods for surgical implants are based on the traditional structures made of titanium alloys and cobalt-chromium alloys, without considering the influence of porosity and degradation, thus precluding the full potential of AM and degradable metals from wide adoption. As for degradable metals, the dynamic mechanical properties of Mg implants change constant during degradation and bone growth. Furthermore, degradation is a chemical reaction from the surface to the bulk and the geometry plays a key role in the degradation behavior. In theory, a porous structure has a large surface area and undergoes fast degradation that affects the inherent mechanical properties and biocompatibility. Therefore, optimization of the structural optimization design and efficacy of Mg-based metal surgical implants is necessary in order to fully exploit the design flexibility of AM and investigate the impact of materials degradation on the structural integrity, mechanical bearing capacity, and biocompatibility of orthopedic repair products in order to accomplish comprehensive performance control and adaptation of different parts of the product in the future. Firstly, Since the physical and chemical properties of 3D printed Mg-based medical devices are interrelated, each property is influenced and controlled by multiple factors and it is difficult and time consuming to quantify the connection between these factors by traditional methods. The proper models can be established by neural networks, big data, artificial intelligence, machine learning, and other computational methods to optimize the product structure. Secondly, customized, porous, and functional gradient bionic design and efficacy evaluation must be carried out to meet the clinical needs and a comprehensive database based on experimental data and artificial intelligence should be established to aid future design.

5.5. Degradation and biocompatibility study of biomedical AM Mg-based products

Regardless of which AM process is implemented to produce Mg-based metal surgical implants, the microstructures, mechanical properties, degradation rate, biocompatibility, and other properties are bound to be different from those of products prepared by conventional processes [174]. At present, there are still many unsolved questions about the safety and *in vivo* absorption and metabolism of the AM products, especially the genotoxicity, carcinogenicity, and reproductive toxicity during the service lifetime of the implants *in vivo* [20]. The latest standard "Qualitative and quantitative degradation products of metals and alloys" (ISO 10,993.15:2019), which is being revised and will be promulgated soon in China, clearly states: "The available electrochemical methods may not be able to accurately reflect the degradation behaviors of the degradable implants in the biological environment, and do not provide the detailed requirements regarding acceptable levels of degradation products. The new immersion tests added to the standard also point out that the different electrolytes chosen for degradable metals will significantly affect their degradation rates and degradation products, and that factors affecting corrosion results include the volume of solution to specimen specific surface area (V/S), flow rate, immersion time, and corrosion rate evaluation methods, of which the selection of appropriate simulated solutions and V/S ratios is particularly critical."

In the actual evaluation of the degradation characteristics of Mg alloy medical devices, the pH, dissolved gas, fluid flow rate, mass loss, degradation products, and hydrogen release should be considered [177]. Compared to compact 3D printed products, the *in vivo* data of porous AM Mg-based metals and composites are inadequate, and more evaluation is needed concerning the safety, efficiency, and cost in order to be commercially competitive. Therefore, there is an urgent need to devise systematic, comprehensive, accurate, effective, and reliable tests and evaluation methods to monitor the degradation, absorption, and metabolism of degradable Mg alloy surgical implants *in vivo* prior to clinical application.

5.6. Surface modification and protection of biomedical AM Mg-based products

The key to achieving personalized biodegradable Mg surgical implants is to regulate the rate of degradation to be compatible with tissue repair. Mg-based materials degrade more swiftly than other metals such as zinc alloys and iron. Although multi-component Mg alloy systems and supporting manufacturing processes have been developed, most of them are applicable only to traditional manufacturing of Mg-based block materials and there have been few systematic studies

on surface modification and degradation of porous Mg-based implants.

Although the dimensional accuracy of powder laser AM products is relatively high, there are inevitable dimensional errors between the porous printed molded parts and design parameters. A rougher surface created by surface powder adhesion can impact the degradation behavior and there are similar problems with wire arc printed products. Therefore, in addition to optimizing the alloy composition, improving the quality of the printing powders and wires, enhancing the design of the product structure, and improving the AM process by surface modification is also essential [178]. Surface modification or surface treatment such as sand blasting, mechanical and chemical polishing, surface alloying, and surface coating or plating can effectively improve the surface quality of the products, including mechanical, degradable, antibacterial and anti-inflammatory characteristics [110,179]. Hence, it is necessary to investigate the influence of the geometry of the porous Mg-based implants and the surface modification on the mechanical properties, degradation properties, and biological functions to fully reveal the degradation behavior *in vivo* and influence mechanisms on cell adhesion, proliferation, and growth.

5.7. Clinical applications of AM Mg-based materials

Biodegradable Mg alloy implants such as vascular stents, bone plates, and bone screws have been shown to produce encouraging clinical results [180,181]. However, clinical adoption of AM biomedical Mg-based products has just started and no actual products are available on the market. However, it is foreseeable that utilizing powder laser AM to manufacture personalized porous structures for surgical implants such as rods, nails, and blocks, will be promising in order to achieve clinical breakthroughs pertaining to the repair and treatment of localized bone defects caused by orthopedic trauma such as bone tumors resection and comminuted fractures [23].

Although AAM is mainly used for efficient and high-quality forming of industrial parts with simple structure, AAM shows large potential in rapid prototyping of products with fine and high complexity [68,174]. In addition, since the raw materials for AAM are wires, multi-strand wires or multi-component wires can be used to print 3D products with different chemical compositions and tissue properties for different stacking parts in order to achieve holistic manufacturing of heterogeneous materials and multifunctional gradient components [78]. Hence, in the future, it is possible to produce high-end medical devices with complex structures and special functions such as artificial femurs, artificial joints, and spines made from Mg-based bioceramic composites for human bone tissue replacement.

The degradation rates of Mg-based implants should match the regeneration and reconstruction rates of bone tissues thus requiring specific designs based on actual clinical needs [172,182]. During the design process, materials selection, structures design, manufacturing process control, and biosafety assessment will pose a formidable interdisciplinary challenge demanding the cooperation and expertise of researchers in various fields including materials science, mechanical engineering, surface science, information technology, equipment engineering, biology, medicine, and imaging. All in all, it is undeniable that the future clinical application of additively manufactured biodegradable Mg-based metallic implants has immense potential.

6. Conclusions

The preparation of raw materials, manufacturing process, properties, applications, and future prospects of AM Mg-based biomedical materials are reviewed and discussed in this paper and the conclusions are as follows:

(1) The primary raw materials for Mg-based AM products are Mg powders and wires. Mg powders necessitate consistent sizing, with an optimal particle range of approximately 20∼70 μm, whereas Mg wires processing typically involve large plastic deformation such as hot extrusion, cold drawing, etc. The quality of AM Mg-based products is contingent upon the quality of the raw materials (Mg powders and wires). Owing to the high activity and surface energy, there is room for improvement in the development of high-grade raw materials for Mg-based AM.
(2) LAM, EBAM, WAAM, and SSAM are common AM techniques to produce Mg-based products. LAM has the advantages of high dimensional tolerance and satisfactory strength, but limited ductility, while EBAM molding is akin to LAM. However, the fast heating and cooling effects of high-energy electron beams may produce inherent flaws in the printed components. WAAM produces moderate strength and appreciable ductility, and SSAM shows a higher tool force and velocity leading to an elevated cladding temperature, consequently resulting in higher porosity in the components.
(3) Our present comprehension of the mechanical characteristics, degradation traits, and biocompatibility of Mg-based 3D printed components for biomedical purposes as well as the variables that impact these features is insufficient and further research is required.
(4) Following are the areas requiring future research and development: (i) Standard preparation of high-quality raw materials, (ii) Development of special equipment, (iii) Innovative manufacturing technology, (iv) Optimal structural design, (v) In-depth study of the properties and performance, (vi) Surface modification, and (vii) Clinical applications.

Declaration of competing interest

The authors declare that they have no known competing financial interests or personal relationships that could have appeared to influence the work reported in this paper.

Acknowledgments

This work was financially supported by the Guangdong Basic and Applied Basic Research Foundation (No. 2020B1515120078, 2021A1515111140, and 2021B1515120059), National Key Research and Development Project of China (No. 2020YFC1107202), Science Research Cultivation Program (PY2022002), Science and Technology Planning Project of Guangzhou (No. 202206010030), City University of Hong Kong Donation Research Grants [DONRMG No. 9229021 and 9220061], as well as City University of Hong Kong Strategic Research Grant [SRG 7005505].

References

[1] Y. Chen, Z. Xu, C. Smith, J. Sankar, Acta Biomater 10 (2014) 4561–4573.
[2] B. Wildemann, K.D. Jandt, Materials 14 (2021) 5834.
[3] B. Patel, G. Favaro, F. Inam, M.J. Reece, A. Angadji, W. Bonfield, J. Huang, M. Edirisinghe, Mater Sci Eng C 32 (2012) 1222–1229.
[4] N. Soro, E.G. Brodie, A. Abdal-hay, A.Q. Alali, D. Kent, M.S. Dargusch, Mater Des 218 (2022) 110688.
[5] M. Li, M. Jiang, Y. Gao, Y. Zheng, Z. Liu, C. Zhou, T. Huang, X. Gu, A. Li, J. Fang, Bioact Mater 11 (2022) 140–153.
[6] Q. Fu, W. Li, S. Yu, Z. Yu, Rare Met Mater Eng 50 (2021) 2630–2640.
[7] W. Li, W. Qiao, X. Liu, D. Bian, D. Shen, Y. Zheng, J. Wu, K.Y. Kwan, T.M. Wong, K.M. Cheung, Adv Sci 8 (2021) 2102035.
[8] X. Pei, L. Wu, H. Lei, C. Zhou, H. Fan, Z. Li, B. Zhang, H. Sun, X. Gui, Q. Jiang, Acta Biomater 126 (2021) 485–495.
[9] H. Kolken, C. De Jonge, T. Van der Sloten, A.F. Garcia, B. Pouran, K. Willemsen, H. Weinans, A. Zadpoor, Acta Biomater 125 (2021) 345–357.
[10] B. Jia, Z. Zhang, Y. Zhuang, H. Yang, Y. Han, Q. Wu, X. Jia, Y. Yin, X. Qu, Y. Zheng, Biomaterials 287 (2022) 121663.
[11] D. Xia, F. Yang, Y. Zheng, Y. Liu, Y. Zhou, Bioact Mater 6 (2021) 4186–4208.
[12] Y. Yang, X. Xiong, J. Chen, X. Peng, D. Chen, F. Pan, J Magnes Alloys 9 (2021) 705–747.
[13] H. Wang, H. Yuan, J. Wang, E. Zhang, M. Bai, Y. Sun, J. Wang, S. Zhu, Y. Zheng, S. Guan, Acta Biomater 129 (2021) 323–332.
[14] D. Li, D. Zhang, Q. Yuan, L. Liu, H. Li, L. Xiong, X. Guo, Y. Yan, K. Yu, Y. Dai, Acta Biomater 141 (2022) 454–465.
[15] M.N. Sarian, N. Iqbal, P. Sotoudehbagha, M. Razavi, Q.U. Ahmed, C. Sukotjo, H. Hermawan, Bioact Mater 12 (2022) 42–63.
[16] Q. Fu, C. Wang, C. Wu, Y. Wu, X. Dai, W. Jin, B. Guo, M. Song, W. Li, Z. Yu, J Alloys Compd 927 (2022) 167018.
[17] Z. Chang, Q. Deng, Q. Lan, J. Feng, D. Li, B. Liu, Y. Wu, L. Peng, W. Ding, Mater Sci Eng A 848 (2022) 143287.
[18] Y. Tian, X. She, J. Yu, Z. Tang, R. Zhang, X. Ai, H. Dai, K. Zheng, F. Pan, X. Jiang, Surf Interfaces 37 (2023) 102665.
[19] D.F. Shi, C.Y. Wang, C.M. Cepeda-Jiménez, M.T. Pérez-Prado, Acta Mater 221 (2021) 117442.
[20] B. Praveena, N. Lokesh, A. Buradi, N. Santhosh, B. Praveena, R. Vignesh, Mater Today 52 (2022) 1309–1313.
[21] N. Madhuri, V. Jayakumar, M. Sathishkumar, Mater Today 46 (2021) 8573–8577.
[22] M. Lian, B. Sun, Y. Han, B. Yu, W. Xin, R. Xu, B. Ni, W. Jiang, Y. Hao, X. Zhang, Biomaterials 274 (2021) 120841.
[23] K. V, N. Kumar B, S. Kumar S, V. M, Addit Manuf 55 (2022) 102802.
[24] Y. Wang, P. Fu, N. Wang, L. Peng, B. Kang, H. Zeng, G. Yuan, W. Ding, Engineering 6 (2020) 1267–1275.
[25] S. Gangireddy, B. Gwalani, K. Liu, E.J. Faierson, R.S. Mishra, Addit Manuf 26 (2019) 53–64.
[26] N.A. Zumdick, L. Jauer, L.C. Kersting, T.N. Kutz, J.H. Schleifenbaum, D. Zander, Mater Charact 147 (2019) 384–397.
[27] J. Wang, Y. Li, M. Zhong, H. Zhang, Int J Therm Sci 161 (2021) 106751.
[28] P. Sun, Z.Z. Fang, Y. Zhang, Y. Xia, Jom 69 (2017) 1853–1860.
[29] Z.Z. Fang, J.D. Paramore, P. Sun, K.S.R. Chandran, Y. Zhang, Y. Xia, F. Cao, M. Koopman, M. Free, Int Mater Rev 63 (2018) 407–459.
[30] G. Chen, S.Y. Zhao, P. Tan, J. Wang, C.S. Xiang, H.P. Tang, Powder Technol 333 (2018) 38–46.
[31] G. Gong, J. Ye, Y. Chi, Z. Zhao, Z. Wang, G. Xia, X. Du, H. Tian, H. Yu, C. Chen, J Mater Res Technol 15 (2021) 855–884.
[32] J. Tang, Y. Nie, Q. Lei, Y. Li, Adv Powder Technol 30 (2019) 2330–2337.
[33] K. Wei, R. Hu, D. Yin, L. Xiao, S. Pang, Y. Cao, H. Zhou, Y. Zhao, Y. Zhu, Acta Mater 206 (2021) 116604.
[34] K. Zhang, Z. Shao, C.S. Daniel, M. Turski, C. Pruncu, L. Lang, J. Robson, J. Jiang, Mater Sci Eng A 807 (2021) 140821.
[35] Y. Wang, F. Li, N. Bian, H.Q. Du, P. Da Huo, J Magnes Alloys (2021), doi:10.1016/j.jma.2021.08.035.
[36] Y. Tian, H. Miao, J. Niu, H. Huang, B. Kang, H. Zeng, W. Ding, G. Yuan, Trans Nonferrous Met Soc China 31 (2021) 2615–2625.
[37] J. Peng, Z. Zhang, H. Cheng, L. Chen, Q. Zang, S. Lu, T. Guo, W. Zhou, Y. Wu, Mater Sci Eng A 832 (2022) 142437.
[38] D. Zhiming, W. Dayu, Z. Hongjuan, Rare Met Mater Eng 47 (2018) 1655–1661.
[39] M.V. Naik, N. Narasaiah, P. Chakravarthy, R.A. Kumar, Mater Today 56 (2022) 1432–1439.
[40] S. Lee, S. Lee, B. Kim, J Mater Process Technol 210 (2010) 776–783.
[41] Y. Zhang, T. Yang, L. Wang, F. Wang, Mod Manuf Eng 474 (2020) 105.
[42] J. Chen, D.P. Yeh, J. Lee, C. Chen, C. Huang, S.D. Lee, C. Chen, T.B.J. Kuo, C. Kao, C. Kuo, J Strength Cond Res 25 (2011).
[43] Y. Ma, Z. Zhang, C. Xu, J. Zhang, T. Lv, B. Wang, Ordnance Mater Sci Eng 35 (2012) 46–49.
[44] A. Milenin, P. Kustra, Arch Metall Mater 58 (2013) 55–62.
[45] N. Manam, W. Harun, D. Shri, S. Ghani, T. Kurniawan, M.H. Ismail, M. Ibrahim, J Alloys Compd 701 (2017) 698–715.
[46] Z. Zeng, M. Salehi, A. Kopp, S. Xu, M. Esmaily, N. Birbilis, J Magnes Alloys 10 (2022) 1511–1541.
[47] S.M. Thompson, L. Bian, N. Shamsaei, A. Yadollahi, Addit Manuf 8 (2015) 36–62.
[48] Z. Zhu, C. Chen, M. Zhang, Laser Optoelectron P 56 (2019) 190006.
[49] L. Zhang, H. Attar, Adv Eng Mater 18 (2016) 463–475.
[50] C. Ng, M. Savalani, M. Lau, H.C. Man, Appl Surf Sci 257 (2011) 7447–7454.
[51] C. Shuai, L. Liu, M. Zhao, P. Feng, Y. Yang, W. Guo, C. Gao, F. Yuan, J Mater Sci Technol 34 (2018) 1944–1952.
[52] K. Wei, Z. Wang, X. Zeng, Acta Metall Sin 52 (2016) 184–190.
[53] X. Li, X. Liu, S. Wu, K. Yeung, Y. Zheng, P.K. Chu, Acta Biomater 45 (2016) 2–30.
[54] C. He, S. Bin, P. Wu, C. Gao, P. Feng, Y. Yang, L. Liu, Y. Zhou, M. Zhao, S. Yang, Metals 7 (2017) 105.
[55] H. Li, Y. Yu, Y. Li, F. Lin, Addi Manuf 50 (2022) 102579.
[56] C. Guo, P. Zhang, F. Lin, Ind Technol Innov 4 (2017) 6–14.
[57] L.C. Zhang, Y. Liu, S. Li, Y. Hao, Advanced Engineering Materials 20 (2018) 1700842.
[58] B. Li, L. Wang, B. Wang, D. Li, J. Oliveira, R. Cui, J. Yu, L. Luo, R. Chen, Y. Su, Mater Sci Eng A 843 (2022) 143135.
[59] Y. Zhang, W. Jarosinski, Y.G. Jung, J. Zhang, Addit Manuf (2018) 39–51.
[60] Y. Chen, X. Chen, M. Jiang, Z. Lei, Z. Wang, J. Liang, S. Wu, S. Ma, N. Jiang, Y. Chen, J Mater Res Technol 20 (2022) 2578–2590.
[61] Y. Luo, Appl Math Model 37 (2013) 6177–6182.
[62] J. Zhao, B. Zhang, X. Li, R. Li, J Mater Process Technol 220 (2015) 243–250.
[63] S. Zhang, Microstructure and menchanical properties of AZ31 magnesium alloy depostited by electron beam wire fusing deposition, Harbin Institute of Technology, 2019.

[64] M. Sabzi, S.M. Anijdan, A.B. Chalandar, N. Park, H. Jafarian, A. Eivani, Mater Sci Eng A 840 (2022) 142877.
[65] L. Nele, G. Mattera, M. Vozza, Appl Sci 12 (2022) 3615.
[66] J. Li, Y. Qiu, J. Yang, Y. Sheng, Y. Yi, X. Zeng, L. Chen, F. Yin, J. Su, T. Zhang, X. Tong, B. Guo, J Magnes Alloys (2021), doi:10.1016/j.jma.2021.04.007.
[67] M. Srivastava, S. Rathee, A. Tiwari, M. Dongre, Mater Chem Phys 294 (2022) 126988.
[68] B. Tomar, S. Shiva, T. Nath, Mater Today Commun 31 (2022) 103739.
[69] Z. Zhou, H. Shen, B. Liu, W. Du, J. Jin, J Manuf Process 64 (2021) 960–971.
[70] X. Wang, A. Wang, K. Wang, Y. Li, Rapid Prototyping J 25 (2019) 809–819.
[71] S. Zhou, H. Xie, J. Ni, G. Yang, L. Qin, X. Guo, J Manuf Process 82 (2022) 159–173.
[72] J. Norrish, J. Polden, I. Richardson, J Phys D 54 (2021) 473001.
[73] V. Subravel, G. Padmanaban, V. Balasubramanian, Trans Indian Inst Met 68 (2015) 353–362.
[74] V. Subravel, G. Padmanaban, V. Balasubramanian, Nonferrous Met Soc China 24 (2014) 2776–2784.
[75] G. Padmanaban, V. Balasubramanian, Nonferrous Met Soc China 21 (2011) 467–476.
[76] J. Guo, Y. Zhou, C. Liu, Q. Wu, X. Chen, J. Lu, Materials (2016).
[77] X. Yang, J. Liu, Z. Wang, X. Lin, F. Liu, W. Huang, E. Liang, Mater Sci Eng A 774 (2020) 138942.
[78] P. Wang, H. Zhang, H. Zhu, Q. Li, M. Feng, J Mater Process Technol 288 (2021) 116895.
[79] S. Ríos, P.A. Colegrove, F. Martina, S.W. Williams, Addit Manuf 21 (2018) 651–657.
[80] S. Han, M. Zielewski, D. Martinez Holguin, M. Michel Parra, N. Kim, Appl Sci 8 (2018) 1306.
[81] W.D. Hartley, D. Garcia, J.K. Yoder, E. Poczatek, J.H. Forsmark, S.G. Luckey, D.A. Dillard, H.Z. Yu, J Mater Process Technol 291 (2021) 117045.
[82] H.Z. Yu, M.E. Jones, G.W. Brady, R.J. Griffiths, D. Garcia, H.A. Rauch, C.D. Cox, N. Hardwick, Scr Mater 153 (2018) 122–130.
[83] V. Gopan, K.L.D. Wins, A. Surendran, J Manuf Sci Tec 32 (2021) 228–248.
[84] S. Palanivel, P. Nelaturu, B. Glass, R.S. Mishra, Mater Des 65 (2015) 934–952.
[85] S. Wlodarski, D.Z. Avery, B.C. White, C.J.T. Mason, C. Cleek, M.B. Williams, P.G. Allison, J.B. Jordon, J Mater Eng Perform 30 (2021) 964–972.
[86] Y. Li, B. Yang, T. Han, Z. Chu, L. Tuo, C. Xue, Q. Yang, X. Zhao, H. Gao, Mater Sci Eng A 845 (2022) 143234.
[87] Z. Wang, T. Wang, Y. Guan, L. Zhu, Mater Sci Eng A 804 (2021) 140794.
[88] Y. Ho, K. Man, S.S. Joshi, M.V. Pantawane, T. Wu, Y. Yang, N.B. Dahotre, Bioact Mater 5 (2020) 891–901.
[89] Y.-H. Ho, S.S. Joshi, T.-C. Wu, C.-M. Hung, N.-J. Ho, N.B. Dahotre, Mater Sci Eng C 109 (2020) 110632.
[90] Y. Zheng, D. Xia, Y. Shen, Y. Liu, Y. Xu, P. Wen, Y. Tian, Y. Lai, Acta Metall Sin 57 (2021) 1499–1520.
[91] F. Witte, V. Kaese, H. Haferkamp, E. Switzer, A. Meyer-Lindenberg, C.J. Wirth, H. Windhagen, Biomaterials 26 (2005) 3557–3563.
[92] H. Windhagen, K. Radtke, A. Weizbauer, J. Diekmann, Y. Noll, U. Kreimeyer, R. Schavan, C. Stukenborg-Colsman, H. Waizy, BioMed Eng online 12 (2013) 1–10.
[93] J. Lee, H. Han, K. Han, J. Park, H. Jeon, M. Ok, H. Seok, J. Ahn, K.E. Lee, D. Lee, Proc Natl Acad Sci 113 (2016) 716–721.
[94] D. Zhao, F. Witte, F. Lu, J. Wang, J. Li, L. Qin, Biomaterials 112 (2017) 287–302.
[95] C. Ng, M. Savalani, H.C. Man, I. Gibson, Virtual Phys Prototy 5 (2010) 13–19.
[96] L. Jauer, W. Meiners, S. Vervoort, C. Gayer, N.A. Zumdick, D. Zander, in: European PM Conference Proceedings, The European Powder Metallurgy Association, 2016, pp. 1–6.
[97] Y. Li, J. Zhou, P. Pavanram, M.A. Leeflang, L.I. Fockaert, B. Pouran, N. Tümer, K.U. Schröder, J.M.C. Mol, H. Weinans, H. Jahr, A.A. Zadpoor, Acta Biomater 67 (2018) 378–392.
[98] K. Xie, N. Wang, Y. Guo, S. Zhao, J. Tan, L. Wang, G. Li, J. Wu, Y. Yang, W. Xu, Bioact Mater 8 (2022) 140–152.
[99] J.H. Martin, B. Yahata, J. Mayer, R. Mone, E. Stonkevitch, J. Miller, R. Mark, T. Schaedler, J. Hundley, P. Callahan, Acta Materialia 200 (2020) 1022–1037.
[100] K. Wei, X. Zeng, Z. Wang, J. Deng, M. Liu, G. Huang, X. Yuan, Mater Sci Eng A 756 (2019) 226–236.
[101] B. Song, S. Dong, Q. Liu, H. Liao, C. Coddet, Mater Des 54 (2014) 727–733.
[102] C. Shuai, Y. Yang, P. Wu, X. Lin, Y. Liu, Y. Zhou, P. Feng, X. Liu, S. Peng, J Alloys Compd 691 (2017) 961–969.
[103] A. Pawlak, M. Rosienkiewicz, E. Chlebus, Arch Civ Mech Eng 17 (2017) 9–18.
[104] T. DebRoy, H. Wei, J. Zuback, T. Mukherjee, J. Elmer, J. Milewski, A.M. Beese, A.d. Wilson-Heid, A. De, W. Zhang, Prog Mater Sci 92 (2018) 112–224.
[105] Y. Qin, P. Wen, H. Guo, D. Xia, Y. Zheng, L. Jauer, R. Poprawe, M. Voshage, J.H. Schleifenbaum, Acta Biomater 98 (2019) 3–22.
[106] B. Guo, M. Song, X. Zhang, Y. Liu, X. Cen, B. Chen, W. Li, Composites Part B 211 (2021) 108646.
[107] C.C. Ng, M.M. Savalani, M.L. Lau, H.C. Man, Appl Surf Sci 257 (2011) 7447–7454.
[108] K. Wei, Z. Wang, X. Zeng, Metall Sin 52 (2016) 184–190.
[109] K. Wei, M. Gao, Z. Wang, X. Zeng, Mater Sci Eng A 611 (2014) 212–222.
[110] X. Niu, H. Shen, J. Fu, J. Feng, Mater Des 206 (2021) 109787.
[111] S. Liu, W. Yang, X. Shi, B. Li, S. Duan, H. Guo, J. Guo, J Alloys Compd 808 (2019) 151160.
[112] C. Shuai, L. Liu, M. Zhao, P. Feng, Y. Yang, W. Guo, C. Gao, F. Yuan, J Mater Res Technol 34 (2018) 1944–1952.
[113] Y. Zhou, P. Wu, Y. Yang, D. Gao, P. Feng, C. Gao, H. Wu, Y. Liu, H. Bian, C. Shuai, J Alloys Compd 687 (2016) 109–114.
[114] Q. Deng, Y. Wu, N. Su, Z. Chang, J. Chen, L. Peng, W. Ding, Addit Manuf 44 (2021) 102036.
[115] A. Kopp, T. Derra, M. Müther, L. Jauer, J.H. Schleifenbaum, M. Voshage, O. Jung, R. Smeets, N. Kröger, Acta Biomater 98 (2019) 23–35.
[116] J. Bi, J. Shen, S. Hu, Y. Zhen, F. Yin, X. Bu, Mater Lett 276 (2020) 128185.
[117] Y. Guo, H. Pan, L. Ren, G. Quan, Mater Lett 247 (2019) 4–6.
[118] Y.F. Zheng, X.N. Gu, F. Witte, Mater Sci Eng R 77 (2014) 1–34.
[119] M.U. Arshad, D. Dutta, Y.Y. Sin, S.W. Hsiao, C.Y. Wu, B.K. Chang, L. Dai, C.Y. Su, Carbon 195 (2022) 141–153.
[120] Y. Lu, A. Bradshaw, Y.-L. Chiu, I. Jones, Mater Sci Eng C 48 (2015) 480–486.
[121] B. Feng, G. Liu, P. Yang, S. Huang, D. Qi, P. Chen, C. Wang, J. Du, S. Zhang, J. Liu, J Magnes Alloys 10 (2022) 1598–1608.
[122] S. Ahmadi, R. Kumar, E. Borisov, R. Petrov, S. Leeflang, Y. Li, N. Tümer, R. Huizenga, C. Ayas, A. Zadpoor, Acta Biomater 83 (2019) 153–166.
[123] Y. Li, H. Jahr, X. Zhang, M. Leeflang, W. Li, B. Pouran, F. Tichelaar, H. Weinans, J. Zhou, A. Zadpoor, Addit Manuf 28 (2019) 299–311.
[124] Y. Li, W. Li, F. Bobbert, K. Lietaert, J. Dong, M. Leeflang, J. Zhou, A. Zadpoor, Acta Biomater 106 (2020) 439–449.
[125] Y. Li, K. Lietaert, W. Li, X. Zhang, M. Leeflang, J. Zhou, A. Zadpoor, Corros Sci 156 (2019) 106–116.
[126] C. Shuai, Y. Zhou, Y. Yang, P. Feng, L. Liu, C. He, M. Zhao, S. Yang, C. Gao, P. Wu, Materials 10 (2017) 307.
[127] Y. Liu, Y. Zheng, X. Chen, J. Yang, H. Pan, D. Chen, L. Wang, J. Zhang, D. Zhu, S. Wu, Adv Funct Mater 29 (2019) 1805402.
[128] P. Saha, M. Roy, M.K. Datta, B. Lee, P.N. Kumta, Mater Sci Eng C 57 (2015) 294–303.
[129] J. Venezuela, M. Dargusch, Acta Biomater 87 (2019) 1–40.
[130] N. Sezer, Z. Evis, M. Koc, J Magnes Alloys 9 (2021) 392–415.

[131] X. Wang, S. Xu, S. Zhou, W. Xu, M. Leary, P. Choong, M. Qian, M. Brandt, Y.M. Xie, Biomaterials 83 (2016) 127–141.
[132] L. Zhen, S.A. Creason, F.I. Simonovsky, J.M. Snyder, S.L. Lindhartsen, M.M. Mecwan, B.W. Johnson, J. Himmelfarb, B.D. Ratner, Biomaterials 279 (2021) 121174.
[133] A.A. Vu, D.A. Burke, A. Bandyopadhyay, S. Bose, Addit Manuf 39 (2021) 101870.
[134] A.A. Zadpoor, Biomater Sci 3 (2015) 231–245.
[135] R. Wu, Y. Li, M. Shen, X. Yang, L. Zhang, X. Ke, G. Yang, C. Gao, Z. Gou, S. Xu, Bioact Mater 6 (2021) 1242–1254.
[136] M.N. Collins, G. Ren, K. Young, S. Pina, R.L. Reis, J.M. Oliveira, Adv Funct Mater 31 (2021) 2010609.
[137] P. Moghimian, T. Poirié, M. Habibnejad-Korayem, J.A. Zavala, J. Kroeger, F. Marion, F. Larouche, Addit Manuf 43 (2021) 102017.
[138] L. Xiong, A.C. Chuang, J. Thomas, T. Prost, E. White, I. Anderson, D. Singh, Adv Powder Technol 33 (2022) 103486.
[139] R. Karunakaran, S. Ortgies, A. Tamayol, F. Bobaru, M.P. Sealy, Bioact Mater 5 (2020) 44–54.
[140] C.L. Wu, W. Zai, H.C. Man, Mater Today Commun 26 (2021) 101922.
[141] S. Li, Q. Gao, J. Zhao, H. Li, P. Wang, Z. Yu, Mater China 40 (2021) 130–138.
[142] B. Yin, Y. Qin, P. Wen, Y. Zheng, Y. Tian, Chin J Lasers 47 (2020) 1100001.
[143] D.D. Gu, W. Meiners, K. Wissenbach, R. Poprawe, Int Mater Rev 57 (2012) 133–164.
[144] M. Esmaily, Z. Zeng, A. Mortazavi, A. Gullino, S. Choudhary, T. Derra, F. Benn, F. D'Elia, M. Müther, S. Thomas, Addit Manuf 35 (2020) 101321.
[145] B. Zhang, H. Liao, C. Coddet, Mater Des 34 (2012) 753–758.
[146] J. Ge, J. Lin, H. Fu, Y. Lei, R. Xiao, Mater Des 160 (2018) 218–228.
[147] S. Yu, R. Yu, T. He and Y. Dai, *Mater China*, **3**, 2021, 198–209.
[148] H. Tiismus, A. Kallaste, T. Vaimann, A. Rassõlkin, Addit Manuf 55 (2022) 102778.
[149] M. Grasso, A.G. Demir, B. Previtali, B.M. Colosimo, Robot Cim-Int Manuf 49 (2018) 229–239.
[150] W.E. King, A.T. Anderson, R.M. Ferencz, N.E. Hodge, C. Kamath, S.A. Khairallah, A.M. Rubenchik, Appl Phys Rev 2 (2015) 041304.
[151] T. Lu, C. Liu, Z. Li, Q. Wu, J. Wang, T. Xu, J. Liu, H. Wang, S. Ma, J Alloys Compd 817 (2020) 153334.
[152] Z. Lu, H. Tian, S. Chen, F. Li, Acta Metall Sin 56 (2019) 83–98.
[153] T. Régnier, G. Fromentin, B. Marcon, J. Outeiro, A. d'Acunto, A. Crolet, T. Grunder, J Mater Process Technol 257 (2018) 112–122.
[154] D.W. Hutmacher, Biomaterials 21 (2000) 2529–2543.
[155] V.C. Mow, R. Huiskes, Basic orthopaedic biomechanics and Mechano-Biology, Lippincott Williams and Wilkins, 2005.
[156] Y. Li, J. Shi, H. Jahr, J. Zhou, A.A. Zadpoor, L. Wang, JOM 73 (2021) 4188–4198.
[157] C. Liu, M. Zhang, C. Chen, Mater Sci Eng A 703 (2017) 359–371.
[158] Y. Wang, H. Huang, G. Jia, H. Zeng, G. Yuan, Acta Biomater 135 (2021) 705–722.
[159] Z. Yu, X. Wang, B. Guo, Q. Fu, M. Feng, 2022. CN112916876A.
[160] S.C. Cox, P. Jamshidi, N.M. Eisenstein, M.A. Webber, H. Burton, R.J. Moakes, O. Addison, M. Attallah, D.E. Shepherd, L.M. Grover, ACS Biomater Sci Eng 3 (2017) 1616–1626.
[161] Y. Guo, G. Quan, M. Celikin, L. Ren, Y. Zhan, L. Fan, H. Pan, J Magnes Alloys 10 (2022) 1930–1940.
[162] E. Hosseini, V. Popovich, Addit Manuf 30 (2019) 100877.
[163] S.F.S. Shirazi, S. Gharehkhani, M. Mehrali, H. Yarmand, H.S.C. Metselaar, N.A. Kadri, N.A.A. Osman, Sci Technol Adv Mater 16 (2015) 033502.
[164] V. Manakari, G. Parande, M. Gupta, Metals 7 (2016) 2.
[165] X. Fang, J. Yang, S. Wang, C. Wang, K. Huang, H. Li, B. Lu, J Mater Process Technol 300 (2022) 117430.
[166] T. Klein, A. Arnoldt, M. Schnall, S. Gneiger, JOM 73 (2021) 1126–1134.
[167] Z. Yan, Q. Hu, F. Jiang, S. Lin, R. Li, S. Chen, Addit Manuf 67 (2023) 103504.
[168] M. Gong, Y. Meng, S. Zhang, Y. Zhang, X. Zeng, M. Gao, Addit Manuf 33 (2020) 101180.
[169] K. Hao, Y. Gao, L. Xu, Y. Han, L. Zhao, W. Ren, Mater Sci Eng A 857 (2022) 144093.
[170] S. Duan, Y. Lin, C. Zhang, Y. Li, D. Zhu, J. Wu, W. Lei, Nano Energy 91 (2022) 106650.
[171] Y. Zhu, T. Tang, S. Zhao, D. Joralmon, Z. Poit, B. Ahire, S. Keshav, A.R. Raje, J. Blair, Z. Zhang, Addit Manuf 52 (2022) 102682.
[172] Z. Jia, X. Xu, D. Zhu, Y. Zheng, Prog Mater Sci 134 (2023) 101072.
[173] Y. Li, C. Su, J. Zhu, Results Eng 13 (2022) 100330.
[174] C. Zhang, Z. Li, J. Zhang, H. Tang, H. Wang, J Magnes Alloys 11 (2023) 425–461.
[175] C. Xia, Z. Pan, J. Polden, H. Li, Y. Xu, S. Chen, Y. Zhang, J Manuf Syst 57 (2020) 31–45.
[176] J. Xu, T. Zhang, X. Li, Materials 16 (2023) 3340.
[177] W. Jin, G. Wu, H. Feng, W. Wang, X. Zhang, P.K. Chu, Corros Sci 94 (2015) 142–155.
[178] A.H. Beyzavi, M. Azadi, M. Azadi, S. Dezianian, V. Talebsafa, Mater Lett 337 (2023) 133935.
[179] A.S. Gnedenkov, S.L. Sinebryukhov, V.S. Filonina, N.G. Plekhova, S.V. Gnedenkov, J Magnes Alloys 10 (2022) 3589–3611.
[180] G. Wu, J.M. Ibrahim, P.K. Chu, Surf Coat Technol 233 (2013) 2–12.
[181] Q. Fu, M. Feng, J. Li, N. He, W. Li, J. Li, J. Yang, W. Jin, W. Li, Z. Yu, J Coat Technol Res 19 (2022) 1757–1771.
[182] M. Feng, Q. Fu, J. Li, J. Li, Q. Wang, X. Liu, W. Jin, W. Li, P.K. Chu, Z. Yu, Colloids Surf A 642 (2022) 128647.